

Detecting Localized Categorical Attributes on Graphs

Siheng Chen, *Student Member, IEEE*, Yaoqing Yang, *Student Member, IEEE*, Shi Zong, Aarti Singh, Jelena Kovačević, *Fellow, IEEE*

Abstract—Do users from Carnegie Mellon University form social communities on Facebook? Do signal processing researchers from tightly collaborate with each other? Do Chinese restaurants in Manhattan cluster together? These seemingly different problems share a common structure: an attribute that may be localized on a graph. In other words, nodes activated by an attribute form a subgraph that can be easily separated from other nodes. In this paper, we thus focus on the task of detecting localized attributes on a graph. We are particularly interested in categorical attributes such as attributes in online social networks, ratings in recommender systems and viruses in cyber-physical systems because they are widely used in numerous data mining applications. To solve the task, we formulate a statistical hypothesis testing problem to decide whether a given attribute is localized or not. We propose two statistics: graph wavelet statistic and graph scan statistic, both of which are provably effective in detecting localized attributes. We validate the robustness of the proposed statistics on both simulated data and two real-world applications: high air-pollution detection and keyword ranking in a co-authorship network collected from IEEE Xplore. Experimental results show that the proposed graph wavelet statistic and graph scan statistic are effective and efficient.

Index Terms—attribute graph, graph wavelet basis, graph scan statistic, ranking

I. INTRODUCTION

Massive amounts of data being generated from various sources including social networks, citation, biological, and physical infrastructure have spurred the emerging area of analyzing data supported on graphs [1], [2] giving rise to a variety of scientific and engineering studies; for example, selecting representative training data to improve semi-supervised learning with graphs [3]; detecting communities in communication or social networks [4]; ranking the most important websites on the Internet [5]; and detecting anomalies in sensor networks [6].

Graph signal processing is a theoretical framework for the analysis of high-dimensional data with complex, irregular structure [7], [8]. It extends classical signal processing concepts such as signals, filters, Fourier transform, frequency response, low- and highpass filtering, from signals residing on regular lattices to data residing on general graphs; for example, a graph signal models the data value assigned to each node in a graph. Recent work involves sampling for graph signals [9], [10], [11], [12], recovery for graph signals [13], [14], [15], [16], representations for graph signals [17], [18], uncertainty

S. Chen (sihenc@andrew.cmu.edu), Y. Yang (yaoqingy@andrew.cmu.edu) and S. Zong (szong@andrew.cmu.edu) are with the Dept. of Electrical and Computer Engineering, A. Singh (aarti@cs.cmu.edu) is with the Dept. of Machine Learning and J. Kovačević (jelenak@cmu.edu) is with the Depts. of Electrical and Computer Engineering and Biomedical Engineering, Carnegie Mellon University, Pittsburgh, PA.

The authors gratefully acknowledge support from the NSF through awards 1130616 and 1421919 and the University Transportation Center grant DTRT12-GUTC11 from the US Dept. of Transportation.

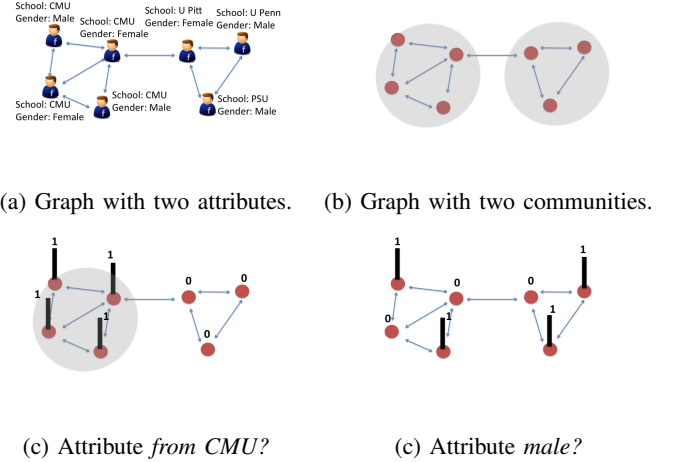


Fig. 1: Detecting localized categorical attributes. (a) Graph with two attributes. (b) Graph with two communities. (c) Attribute *Is this user from CMU?* is localized. (d) Attribute *Is this user male?* is not localized. The goal of community detection is to identify subgraphs as in (b), while the goal of the localized attribute detection is to identify whether an attribute is localized (yes in (c), no in (d)).

principles on graphs [19], [20], stationary graph signal processing [21], [22], graph dictionary construction [23], graph-based filter banks [24], [25], [26], [27], denoising on graphs [24], [28], community detection and clustering on graphs [29], [30], [31], distributed computing [32], [33] and graph-based transforms [34], [35], [36].

We here consider detecting *localized categorical attributes* on graphs. A categorical attribute is defined as a variable that can be put into a countable number of categories. It can be represented by several binary attributes and is widely used in data and graph mining applications [37]. We model categorical attributes by binary graph signals¹: when a signal coefficient is one, the corresponding node is activated by the attribute, and vice versa. A localized categorical attribute, or a localized pattern, is defined as an attribute whose activated nodes form a subgraph that can be easily separated from the rest of nodes; in other words, the cut cost is small. In practice, detecting a localized attribute is nontrivial because an observed attribute is often corrupted by noise. The goal of localized attribute detection is to identify localized attributes hidden in noisy attributes using graph topology. This task is relevant to many real-world applications such as identifying localized attributes in online social networks, activity in the brain connectivity

¹Attributes and binary graph signals are the same in this context.

networks and viruses in cyber-physical systems.

This localized attribute detection task is related to, yet different from conventional community detection in network science [38], [4], [39]. The goal of community detection is to identify modules and hierarchical organization by using the information encoded in the *graph topology only* [40]. A module is typically considered to be a node set with dense internal and sparse external connections. The difference between the two is that community detection considers detecting patterns in graph topology while localized attribute detection considers detecting patterns in an attribute (binary graph signal). For example, suppose that we want to identify whether users from Carnegie Mellon University (CMU) form a localized attribute on Facebook. The binary answer to *Is this user from CMU?* is an attribute on a graph, which activates a subgraph with few external connections. These activated users thus form a localized attribute; see Figure 1.

To describe the localization level of an attribute, we consider external connections of the subgraph activated by the attribute, leading to scalable detection algorithms. We define the localization level of a localized attribute as the difficulty of separating the corresponding subgraph from the rest of the nodes, which is quantified by the total variation on graphs. We then formulate a hypothesis testing problem to decide whether a categorical attribute is localized and propose two statistics: graph wavelet statistic and graph scan statistic. Similarly to detecting transient changes in time-series signals by using wavelet techniques, we design a graph wavelet statistic based on a Haar-like graph wavelet basis. Since the graph wavelet basis is preconstructed, the computational cost is linear with the number of nodes. We also formulate a generalized likelihood test and propose a graph scan statistic, which can be efficiently solved by a standard graph-cut algorithm. The intuition behind the proposed statistics is to find the underlying localized attribute in a graph, which is equivalent to denoising the given attribute based on the graph structure, and then calculating the statistic values based on the denoised attribute. We demonstrate the effectiveness and robustness of the proposed methods through validation on simulated and real data.

We here consider only one attribute per test; when given multiple attributes, we can rank their localization levels according to the proposed statistics. Note that the proposed statistics does not address correlation among attributes.

Contributions. The main contributions of the paper are:

- A novel hypothesis testing framework for *detecting localized attributes* corrupted by Bernoulli noise;
- A novel, effective, and scalable *graph wavelet statistic* for detecting localized attributes with analysis of detection error;
- A novel, effective, and scalable *graph scan statistic* for detecting localized attributes with analysis of detection error; and
- Validation on both *simulated and real datasets* with applications to detection of high air pollution and ranking keywords in a co-authorship network.

Paper outline. Section II formulates the problem; Section III reviews related work; Section IV proposes graph wavelet and scan statistics; Section V validates the proposed methods on

simulated and real data; and Section VI concludes the paper.

II. PROBLEM FORMULATION

We consider a weighted, undirected graph $G = (\mathcal{V}, \mathcal{E}, A)$, with $\mathcal{V} = \{v_1, \dots, v_N\}$ the set of nodes, $\mathcal{E} = \{e_1, \dots, e_M\}$ the set of edges and $A \in \mathbb{R}^{N \times N}$ a weighted adjacency matrix. A *graph signal* is defined as the map that assigns the signal coefficient $s_n \in \mathbb{R}$ to the graph node v_n ; it can be written as a vector $\mathbf{s} = [s_1 \ \dots \ s_N]^T \in \mathbb{R}^N$. The edge weight $A_{i,j}$ between nodes v_i and v_j quantifies the underlying relation between the i th and the j th signal coefficients, such as a similarity, a dependency, or a communication pattern. In this paper, all graph signals are binary ($\mathbf{s} \in \{0, 1\}^N$) and represent attributes; we thus use the word *attribute* instead of *binary graph signal* in what follows.

Let $\Delta \in \mathbb{R}^{|\mathcal{E}| \times |\mathcal{V}|}$ be the *graph incidence matrix*, whose rows correspond to edges [41], [42]; for example, if e_i is the edge that connects the j th node to the k th node ($j < k$), the elements of the i th row of Δ are

$$\Delta_{i,\ell} = \begin{cases} A_{j,k}, & \ell = j; \\ -A_{j,k}, & \ell = k; \\ 0, & \text{otherwise.} \end{cases}$$

An *activated* node set $C \subseteq \mathcal{V}$ is denoted by its indicator function (attribute) $\mathbf{1}_C \in \{0, 1\}^N$,

$$(\mathbf{1}_C)_i = \begin{cases} 1, & v_i \in C; \\ 0, & \text{otherwise.} \end{cases}$$

When C forms a connected subgraph, we call C a *local set*.

We consider the localization level of the attribute $\mathbf{1}_C$ as the difficulty of separating C from $\bar{C} = \mathcal{V} \setminus C$, and use the ℓ_p -norm-based total variation to quantify it,

$$\text{TV}_p(\mathbf{1}_C) = \|\Delta \mathbf{1}_C\|_p. \quad (1)$$

While $\text{TV}_0(\mathbf{1}_C)$ counts the number of edges connecting C and \bar{C} , $\text{TV}_1(\mathbf{1}_C)$ takes edge weights into account; when edges are unweighted, the two are the same. Total variation builds a connection between an attribute and graph structure and measures the localization level of an attribute on a specific graph; that is, an attribute with smaller total variation is more localized on a graph because it is easier to separate its activated part C from its nonactivated part \bar{C} .

The task of localized attribute detection is made harder when noise is present. Given a noisy attribute $\mathbf{y} \in \{0, 1\}^N$, the general statistical testing formulation is:

$$\begin{aligned} H_0^N &: \mathbf{y} \sim f(0, \epsilon), \\ H_1^N &: \mathbf{y} \sim f(\mathbf{s}, \epsilon) \text{ with } \mathbf{s} \in \mathcal{S}_N, \end{aligned} \quad (2)$$

where N indicates that the observation is N -dimensional, with N the number of nodes in the graph, and is independent in each dimension, \mathcal{S}_N is a predefined class of localized attributes, $\epsilon > 0$ is the noise level and the link function $f(\cdot, \cdot)$ specifies the noise model. For example, if a signal is corrupted by Gaussian noise, $f(\mathbf{s}, \epsilon) = \mathbf{s} + \mathbf{e}$, where $\mathbf{e} \sim \mathcal{N}(0, \epsilon \mathbf{I})$.

The null (default) hypothesis thus represents no particular localization for the attribute and the alternative hypothesis represents a localized attribute. The two key factors in (2) are the noise model and the localized attribute, and we can make

independent assumptions on these two. For example, noise can follow Gaussian or Bernoulli distribution and the localization level can be described by small cut costs or cliques [2].

Let the test be a mapping $T(\mathbf{y}) = \{0, 1\}$, where 1 indicates rejecting the null hypothesis. It is imperative that we control both the probability of false positives (incorrectly rejecting a true null hypothesis, *type-1 error*) and false negatives (incorrectly retaining a false null hypothesis, *type-2 error*). We thus define the risk to be

$$R_N(T) = \underbrace{\mathbb{P}(T = 1 | H_0^N \text{ is true})}_{\text{type-1 error}} + \underbrace{\sup_{\mathbf{s} \in \mathcal{S}_N} \mathbb{P}(T = 0 | H_1^N \text{ is true})}_{\text{type-2 error}},$$

where the class of localized attributes \mathcal{S}_N is related to the number of nodes N . Using the definition from [43], [44], [45], we say that H_0^N and H_1^N are *asymptotically distinguishable* by a test T , if $\lim_{N \rightarrow \infty} R_N(T) = 0$. In other words, when the number of nodes goes to infinity and the detection risk goes to zero, H_0^N and H_1^N are asymptotically distinguishable.

Bernoulli noise model. In this paper, we are particularly interested in (2) with the Bernoulli noise model, $f(\mathbf{s}, \epsilon) = \text{Bernoulli}(\mathbf{s} + \epsilon \mathbf{1}_{\mathcal{V}}) \in \mathbb{R}^N$, where each element $f(\mathbf{s}, \epsilon)_i$ is an independent Bernoulli random variable with mean $(\mathbf{s} + \epsilon)_i$,

$$\begin{aligned} H_0^N &: \mathbf{y} \sim \text{Bernoulli}(\epsilon \mathbf{1}_{\mathcal{V}}), \\ H_1^N &: \mathbf{y} \sim \text{Bernoulli}(\mu \mathbf{1}_C + \epsilon \mathbf{1}_{\bar{C}}) \text{ for all } \text{TV}_p(\mathbf{1}_C) \leq \rho, \end{aligned} \quad (3)$$

μ is the activation probability within the localized attribute, ϵ is the noise level and $0 \leq \epsilon < \mu \leq 1$. The number of external edges of a localized attribute, ρ , reflects the shapes of candidate localized attributes and characterizes the alternative hypothesis H_1^N . Here, the average value under H_1^N is larger than the average value under H_0^N . A naive approach is to use the average of the observation as the statistic (see Appendix D). We set the class of localized attributes \mathcal{S}_N to model correlation among nodes as

$$\mathcal{S}_N = \left\{ \mathbf{s} : \mathbf{s} = (\mu - \epsilon) \mathbf{1}_C, C \in \mathcal{C} \right\},$$

with the localized attributes that the user is testing for specified through the class $\mathcal{C} = \{C \subseteq \mathcal{V} : \text{TV}_p(\mathbf{1}_C) \leq \rho\}$, while ρ, p control the cut cost of the activated node set. The cut cost ρ is a user-defined parameter: when ρ is large, all candidate localized attributes are allowed to have any number of external edges and the test always succeeds, while when ρ is small, all candidate localized attributes have few external edges. Note that the Bernoulli model here is similar to the setting in community detection with categorical attributes [46], [37]. For example, suppose that we want to identify whether users who graduated from CMU form a social community on Facebook. The binary value *Is this user from CMU?* is an attribute on Facebook. When this attribute leads to a community, we should find a subgraph such that (1) most nodes are activated within the subgraph and few nodes are activated outside the subgraph; (2) the connection between this subgraph and its complement is weak. *We describe a binary attribute by the Bernoulli noise model and a localized attribute by an attribute with small total-variation.*

III. RELATED WORK

In classical signal processing, a localized signal is constant over local connected regions separated by lower-dimensional boundaries. It is often related to concepts such as impulse function, step function, square wave and Haar basis [47]. Detecting localized signals has been considered through signal/noise discrimination [48], edge detection [49], pattern matching [50] and support recovery of sparse signals [51], [52], among others. We here look at the counterpart problem on graphs. A localized attribute (graph signal) is constant over a subgraph that is easily separated from the rest of the nodes. Similarly to localized signals in classical signal processing, a localized attribute emphasizes fast transitions (corresponding to boundaries) and localization in the graph vertex domain (corresponding to attributes that are nonzero in a local neighborhood).

Our detection problem bears resemblance to many detection problems in the current graph-related literature, such as detecting a smooth graph signal or a localized graph signal under a specific noise model. For example, [43], [53] detects a cluster in a lattice graph that exhibits unusual behavior; [54] constructs a generalized likelihood test to detect smooth graph signals; [55] considers a general graph-structured normal means test; [56] considers combining data gathering and decision-making to design the quickest detection in the Markov random field; [57], constructs the uniform spanning tree wavelet statistic to approximate the epsilon scan statistic; and [44], [45], considers the Lovasz extended scan statistic and spectral relaxation as relaxations of the combinatorial scan statistic.

The uniform spanning tree wavelet statistic and the Lovasz extended scan statistic lay a foundation for this paper; we extend the Gaussian noise model to the Bernoulli one, that is, we deal with binary instead of real values to address categorical attributes. Although one could do this by thresholding a real value, the process leads to information loss. Thus, handling binary-valued attributes is a nontrivial task.

Our detection problem is also related to community detection, which, as one of the key topics in network science and graph mining, aims to extract tightly connected subgraphs in a network, also known as graph partitioning and graph clustering [4], [58], [59]. While the traditional community detection algorithms focus on the graph structure only [38], [60], some recent studies tried to combine the knowledge of both graph structure and node attributes [46] as such attributes not only improve the accuracy of community detection, but also provide the interpretation of detected communities. However, as not all attributes are relevant for all communities, community detection accuracy may suffer. It is also computationally inefficient to include a large number of attributes in the training phase [61]. We here aim to find useful attributes for improving community detection and aiding interpretation; as an example, in Section V, the proposed statistics select useful keywords in a co-authorship network.

IV. METHODOLOGY

We now propose two statistics for testing the hypothesis in (3): graph wavelet statistic and graph scan statistic. The first is based on a graph wavelet basis; when a given attribute has large graph wavelet coefficients, the attribute agrees with

the graph structure and is localized. The second is based on matching all possible node sets to a given attribute via an optimization problem; when we find such a feasible node set, the attribute is localized. The first statistic is more efficient as the graph wavelet basis is pre-constructed, while the second is more accurate as it adaptively searches for localized attributes.

A. Graph Wavelet Statistic

In classical signal processing, one way of detecting a transient change in a time-series signal is by projecting it on the wavelet basis [47]; when a high-frequency coefficient is large, a transient change is present. Similarly, we detect a boundary in a localized attribute by projecting it on a Haar-like graph wavelet basis; when a large graph wavelet coefficient exists in the high-frequency wavelet matrix, the boundary is present, and we reject the null hypothesis.

Similarly to how we construct the Haar basis in classical signal processing [62], we construct the *graph wavelet basis* as in [57], [18]. The idea is to recursively partition each local parent set into two disjoint local child sets of roughly similar sizes, irrespective of the connections between them. We start from the entire node set \mathcal{V} , corresponding to the coarsest resolution in the graph vertex domain, and finish with each local set being either an individual node or an empty set, corresponding to the finest resolution in the graph vertex domain as illustrated in Figure 2. For each partition, a new basis vector \mathbf{w} is added as in Algorithm 1. The decomposition level, or the depth of a decomposition tree, is the maximum number of partitions to reach an individual node. As the proposed decomposition provides a series of redundant local sets with various sizes at various positions, we can either exactly localize attributes or approximate them by using local sets.

Algorithm 1 Local-set-based graph wavelet basis

Input $G(\mathcal{V}, \mathcal{E}, A)$ graph
Output $W \in \mathbb{R}^{N \times N}$ wavelet basis

Function

initialize a stack of node sets \mathbb{S} and a set of basis vectors W
 set $\mathbb{S} = \{S = \mathcal{V}\}$
 set $\mathbf{w}_1 = \frac{1}{\sqrt{|\mathbb{S}|}} \mathbf{1}_S$ as the first column of W
 while the cardinality of the largest element of \mathbb{S} is larger than 1
 take one element from \mathbb{S} at a time as S
 partition S into two disjoint local sets S_1, S_2 by 2-means clustering [18]
 if $|S_1|$ and/or $|S_2|$ is larger than 1, put that local set(s) into \mathbb{S}
 add $\mathbf{w} = \sqrt{\frac{|S_1||S_2|}{|S_1|+|S_2|}} \left(\frac{1}{|S_1|} \mathbf{1}_{S_1} - \frac{1}{|S_2|} \mathbf{1}_{S_2} \right)$ as a new column of W
 return W

To ensure the detection property of the graph wavelet basis, we impose three requirements on each partition: (1) the two local child sets are disjoint; (2) the union of the two local child sets is the local parent set; and (3) the cardinalities of the two local child sets are as close as possible. The first two requirements lead to the orthogonality of the graph wavelet basis while the third promotes the sparsity for all attributes with small ℓ_0 -norm-based total variation. In general, any algorithm that satisfies these three requirements can be used to generate a graph wavelet basis; [18] introduces three such algorithms. Here we use 2-means clustering, which approximately partitions a local set evenly. Inspired by K -means clustering [63],

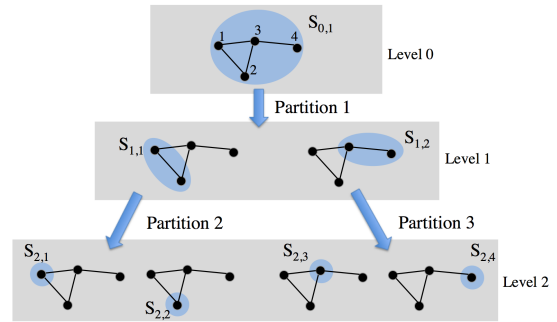


Fig. 2: Wavelet decomposition tree. In each partition, we decompose a local set into two disjoint local sets and generate a wavelet basis vector. For example, in Partition 1, we partition $S_{0,1} = \{1, 2, 3, 4\}$ into $S_{1,1} = \{1, 2\}$, $S_{1,2} = \{3, 4\}$ and generate a wavelet basis vector $[1 \ 1 \ -1 \ -1]/2$. Note that the decomposition is not unique.

for each local set, we select two nodes with the longest geodesic distance from each other as the cluster heads and assign every other node to its nearest cluster head based on the geodesic distance. We then recompute the cluster head for each cluster by minimizing the geodesic distance sum to all other nodes in the cluster and assign node to its nearest cluster head again, until convergence.

The output of Algorithm 1 is the graph wavelet basis $W \in \mathbb{R}^{N \times N}$. It is orthonormal and preserves the energy of any input.

Lemma 1. (Orthogonality [18]) Let W be the output of Algorithm 1. W is an orthonormal basis; that is,

$$W^T W = W W^T = I.$$

We use this graph wavelet basis with balanced splits to construct a sparse representation for localized attributes (which are not communities in general). The upper bound in Lemma 2 below establishes the worst-case scenario, because the graph wavelet basis once constructed is fixed and thus should work for any attribute. The decomposition level L is the bottleneck in a sparse representation and is minimized when we partition each local set evenly, leading to balanced splits.

Lemma 2. (Sparsity [18]) Let W be the output of Algorithm 1 and L be the total decomposition level. For all $\mathbf{y} \in \mathbb{R}^N$,

$$\|W^T \mathbf{y}\|_0 \leq 1 + \|\Delta \mathbf{y}\|_0 L.$$

Combining Lemmas 1 and 2, we see that the graph wavelet representation concentrates the energy of an attribute into a few wavelet coefficients; it is thus indeed a sparse representation,

$$\|W_{(-1)}^T \mathbf{y}\|_\infty^2 \stackrel{(a)}{\geq} \frac{\|W_{(-1)}^T \mathbf{y}\|_2^2}{\|W_{(-1)}^T \mathbf{y}\|_0} \stackrel{(b)}{\geq} \frac{\|\mathbf{y}\|_2^2 - \left(\frac{1}{\sqrt{N}} \mathbf{1}_V^T \mathbf{y}\right)^2}{1 + \|\Delta \mathbf{y}\|_0 L},$$

where $W_{(-1)} \in \mathbb{R}^{N \times (N-1)}$ is W without its first (constant) column as that column only calculates the mean of \mathbf{y} , which is not informative for detection; we call it *high-frequency wavelet matrix*. The inequality (a) follows from the basic norm inequality, and (b) from Lemmas 1 and 2. Theorem 1 will show that the largest nontrivial wavelet coefficient is an important

metric in distinguishing whether \mathbf{y} is a localized attribute or not. We see that the lower bound on that largest nontrivial wavelet coefficient is related to the total decomposition level. To lift the largest nontrivial wavelet coefficient up, we need to minimize the total decomposition level L , which is satisfied with even local set partition, with $L = O(\log_2 N)$. For a localized attribute with a small ℓ_0 -norm-based total variation, the corresponding graph wavelet coefficients are sparse and the energy of the original attribute concentrates in a few graph wavelet coefficients. However, for a noisy attribute with a large ℓ_0 -norm-based total variation, the energy of the original attribute spreads over all graph wavelet coefficients.

The projection of an attribute on a graph wavelet basis vector calculates the absolute difference between its average values on two local node sets (see Algorithm 1); for example, the projection on a basis vector stemming from the partition into S_1 and S_2 is $\sqrt{\frac{|S_1||S_2|}{|S_1|+|S_2|}} \mathbf{y}^T (\mathbf{1}_{S_1}/|S_1| - \mathbf{1}_{S_2}/|S_2|)$. When one local set captures significantly larger average value than the other local set, that local set detects a localized attribute. Because of the multiresolution construction, the graph wavelet basis searches for localized attributes of different sizes. Thus, the maximum value of the graph wavelet coefficient identifies whether the original attribute contains a localized attribute.

We thus define the *graph wavelet statistic* as the maximum absolute value over the high-frequency wavelet coefficients,

$$\hat{w} = \left\| \mathbf{W}_{(-1)}^T \mathbf{y} \right\|_{\infty}, \quad (4)$$

where \mathbf{y} is the noisy observation. When \hat{w} is larger than a threshold, we reject the null hypothesis.

To analyze the graph wavelet statistic, Lemma 3 shows that given a threshold related to the graph size N and a user-defined error tolerance δ , the type-1 error is upper bounded, Theorem 1 shows that when the attribute strength is sufficiently large, both type-1 and type-2 errors can be upper bounded and Corollary 1 states the condition for the asymptotic distinguishability.

Lemma 3. Let the graph wavelet statistic be \hat{w} in (4). Under the statistical test (3) with $p = 0$, we reject the null hypothesis for all $\hat{w} > \tau$, with threshold $\tau = \sqrt{\log N} + \sqrt{2 \log(2/\delta)}$. The corresponding type-1 error is $\mathbb{P}\{T = 1 | H_0^N \text{ is true}\} \leq \delta$.

Theorem 1. Let the attribute strength be sufficiently large,

$$\begin{aligned} \sqrt{|C| \left(1 - \frac{|C|}{N}\right)} (\mu - \epsilon) &\geq \\ \sqrt{1 + \rho \log N} \left(\sqrt{\log N} + \sqrt{2 \log\left(\frac{2}{\delta_1}\right)} + \sqrt{2 \log\left(\frac{2}{\delta_2}\right)} \right). \end{aligned} \quad (5)$$

Then, by using the graph wavelet statistic \hat{w} in Lemma 3, the type-1 error is $\mathbb{P}(T = 1 | H_0^N \text{ is true}) \leq \delta_1$ and the type-2 error is $\mathbb{P}(T = 0 | H_1^N \text{ is true}) \leq 1 - (1 - \delta_2)^4$.

We set $\delta_1 = \delta_2 = 1/N$ to obtain the following corollary.

Corollary 1. Using the graph wavelet statistic \hat{w} in (4), H_0^N and H_1^N are asymptotically distinguishable, that is, $\lim_{N \rightarrow \infty} R_N(T) = 0$, when

$$\sqrt{|C| \left(1 - \frac{|C|}{N}\right)} (\mu - \epsilon) \geq O(\sqrt{\rho} \log N).$$

The proofs of Lemma 3 and Theorem 1 are merged in Appendix A. The main idea is to show that under the null hypothesis, each graph wavelet coefficient is a sub-Gaussian random variable whose distribution is similar to a Gaussian distribution [64], while under the alternative hypothesis, the maximum value of the graph wavelet coefficients is large because the energy of the original attribute concentrates in a few graph wavelet coefficients.

While asymptotic distinguishability in Corollary 1 cannot be evaluated in practice because μ , ϵ and C are unknown, it quantifies the fundamental detection performance of an algorithm and depends on μ , ϵ and C . When the attribute strength is too weak, for example, $\mu = \epsilon$ or $C = 0$, it is impossible for any algorithm to achieve asymptotic distinguishability. In the detection literature, it is common to show that when a predefined signal strength is sufficiently large, the null and alternative hypotheses are asymptotically distinguishable. Theorem 1 and Corollary 1 follow the same path; see other similar examples in [65], [43], [57], [45], [53].

Theorem 1 relates the size of a localized attribute $|C|$, the activation probability difference $\mu - \epsilon$ and asymptotic distinguishability. With a constant $|C|$, it is easier to detect a localized attribute when the activation probability difference $\mu - \epsilon$ is large; with constant μ, ϵ , it is easier to detect a larger localized attribute with a small cut cost ρ . When ρ is large, all candidate localized attributes are allowed to have any number of external edges and a larger $|C|$ is required to increase the attribute strength, while when ρ is small, all candidate localized attributes have few external edges. When $|C|$ is fairly large; that is, $O(N) \gg |C| \gg O(1)$, $(1 - |C|/N)\sqrt{|C|}(\mu - \epsilon)$ asymptotically approximates $\sqrt{|C|}(\mu - \epsilon)$; When $|C|$ is too close to N , the condition (5) fails because the observation \mathbf{y} is close to an all-one vector and most of the energy is captured by the first column vector of the graph wavelet basis, causing a small \hat{w} ; however, in practice we typically consider $|C| \ll O(N)$, because localized attributes are relatively small compared to the entire graph.

Since the distribution of graph wavelet statistic does not have an analytical form, it is hard to calculate the exact p -value. Instead, we use sub-Gaussianity to provide an upper bound on the p -value. Given the graph wavelet statistic \hat{w} in (4), the upper bound on the p -value is $\exp\left(-\frac{1}{2}(\hat{w} - \sqrt{\log N})^2\right)$. Let our test be level α . When α is larger than the upper bound on the p -value, α is definitely larger than the exact p -value. We then reject the null hypothesis for all $\alpha \geq \exp\left(-\frac{1}{2}(\hat{w} - \sqrt{\log N})^2\right)$. The threshold is only related to the size of the graph N .

The computational bottleneck in constructing the graph wavelet basis is the graph partition algorithm from Figure 2. Let the computational cost of the graph partition algorithm be of the order $O(h(N))$, where $h(\cdot)$ is a polynomial function. The total computational cost to construct a graph wavelet basis behaves as $O\left(\sum_{i=0}^{\log N} 2^i h(N/2^i)\right)$; for example, when the cost of a graph partition algorithm is of the order $O(N \log N)$, the total computational cost to construct a graph wavelet basis behaves as $O(N \log^2 N)$. Since the graph wavelet basis is constructed based on the graph structure only, the construction

is performed only once and works for any attribute supported on this graph. The total computational cost to obtain the graph wavelet statistic only involves a matrix-vector multiplication and a search for the maximum value. The graph wavelet statistic is thus scalable to large-scale graphs.

B. Graph Scan Statistic

In the previous subsection, we constructed a graph wavelet statistic to test whether a given attribute is localized. While the graph wavelet statistic is efficient, the construction of the graph wavelet basis does not depend on the attribute. We now propose a data-adaptive approach, which scans all feasible node sets based on a given attribute. The intuition behind the proposed statistics is that given the noisy observation \mathbf{y} , we search for an activated node set C . If we can find such a C , we reject the null hypothesis, and vice versa.

If we knew the true activated node set $C \in \mathcal{C}$, we could test the null hypothesis $H_0^N : \mathbf{s} = 0$ against the alternative $H_1^N : \mathbf{s} = \mu \mathbf{1}_C$ by using the likelihood ratio test. Given the observation \mathbf{y} and the Bernoulli noise model, the likelihood is

$$\mathbb{P}(\mathbf{y}|H_1^N \text{ is true}) = \prod_{i \in C} \mu^{y_i} (1 - \mu)^{1 - y_i} \prod_{i \in \bar{C}} \epsilon^{y_i} (1 - \epsilon)^{1 - y_i},$$

and we estimate the unknown parameters as $\hat{\mu} = \mathbf{1}_C^T \mathbf{y} / |C|$ and $\hat{\epsilon} = \mathbf{1}^T \mathbf{y} / N$. The likelihood ratio is

$$\begin{aligned} & \frac{\prod_{i \in \mathcal{V}} \hat{\epsilon}^{y_i} (1 - \hat{\epsilon})^{1 - y_i}}{\prod_{i \in C} \hat{\mu}^{y_i} (1 - \hat{\mu})^{1 - y_i} \prod_{i \in \bar{C}} \hat{\epsilon}^{y_i} (1 - \hat{\epsilon})^{1 - y_i}} \\ &= \prod_{i \in C} \left(\frac{\hat{\epsilon}}{\hat{\mu}} \right)^{y_i} \left(\frac{1 - \hat{\epsilon}}{1 - \hat{\mu}} \right)^{1 - y_i}. \end{aligned}$$

The log likelihood ratio is

$$\begin{aligned} & \sum_{i \in C} y_i \log \left(\frac{\hat{\epsilon}}{\hat{\mu}} \right) + \sum_{i \in \bar{C}} (1 - y_i) \log \left(\frac{1 - \hat{\epsilon}}{1 - \hat{\mu}} \right) \\ &= |C| \left(\hat{\mu} \log \left(\frac{\hat{\epsilon}}{\hat{\mu}} \right) + (1 - \hat{\mu}) \log \left(\frac{1 - \hat{\epsilon}}{1 - \hat{\mu}} \right) \right) \\ &= -|C| \text{KL}(\hat{\mu} \parallel \hat{\epsilon}), \end{aligned}$$

where $\text{KL}(\cdot \parallel \cdot)$ is the Kullback-Leibler divergence [63].

In practice, however, the true activated node set C is unknown; we then consider the generalized likelihood ratio

$$\hat{g} = \max_C |C| \text{KL} \left(\frac{\mathbf{1}_C^T \mathbf{y}}{|C|} \parallel \frac{\mathbf{1}^T \mathbf{y}}{N} \right) \quad (6)$$

subject to $\text{TV}_1(\mathbf{1}_C) \leq \rho$.

We call \hat{g} *graph scan statistic*. To maximize the objective in (6), the localized attribute C should trade-off between its size $|C|$ and the average value inside $\mathbf{1}_C^T \mathbf{y} / |C|$. When $|C|$ is large, $\mathbf{1}_C^T \mathbf{y} / |C|$ tends to be small; on the other hand, when C fits the activated nodes in \mathbf{y} , $\mathbf{1}_C^T \mathbf{y} / |C|$ is large; however, due to the cut cost constraint, C can only fit a few scattered nodes and $|C|$ is small. The goal of the graph scan statistic is to search for a node set with both large cardinality and large average value.

When \hat{g} is larger than some threshold, we detect an activated node set and reject the null hypothesis. To analyze the graph scan statistic, Lemma 4 shows that given a threshold related to the size of the graph N , a user-defined error tolerance δ

and cut cost ρ , the type-1 error is upper bounded, Theorem 2 shows that when the attribute strength is sufficiently large, both type-1 and type-2 errors can be upper bounded and Corollary 2 states the condition of the asymptotic distinguishability.

Lemma 4. Let the graph scan statistic be \hat{g} in (6). Under the statistical test (3) with $p = 1$, we reject the null hypothesis for all $\hat{g} > \tau$, with

$$\begin{aligned} \tau &= 8 \left(\left(\sqrt{\rho} + \sqrt{\frac{1}{2} \log N} \right) \sqrt{2 \log(N-1)} \right. \\ &\quad \left. + \sqrt{2 \log 2} + \sqrt{\frac{9}{2} \log\left(\frac{2}{\delta}\right)} \right)^2. \end{aligned}$$

The corresponding type-1 error is $\mathbb{P}\{T = 1 | H_0^N \text{ is true}\} \leq 1 - (1 - \delta)^2$.

Theorem 2. Let the attribute strength be sufficiently large,

$$\begin{aligned} \left(1 - \frac{|C|}{N}\right) \sqrt{|C|}(\mu - \epsilon) &\geq \left(4\sqrt{\log 2} + 6\sqrt{\log\left(\frac{2}{\delta_1}\right)} + \right. \\ &4\left(\sqrt{\rho} + \sqrt{\frac{1}{2} \log N}\right) \sqrt{\log(N-1)} + \\ &\left. \left(\sqrt{\frac{1}{2}} + \sqrt{\frac{|C|}{2N}}\right) \sqrt{\log\left(\frac{2}{\delta_2}\right)}\right). \quad (7) \end{aligned}$$

Then, by using the graph scan statistic \hat{g} in Lemma 4, the type-1 error is $\mathbb{P}(T = 1 | H_0^N \text{ is true}) \leq 1 - (1 - \delta_1)^2$ and the type-2 error is $\mathbb{P}(T = 0 | H_1^N \text{ is true}) \leq 1 - (1 - \delta_2)^3$.

We set $\delta_1 = \delta_2 = 1/N$ and obtain the following corollary.

Corollary 2. Using the graph scan statistic \hat{g} in (6), H_0^N and H_1^N are asymptotically distinguishable, that is, $\lim_{N \rightarrow \infty} R_N(T) = 0$, when

$$\left(1 - \frac{|C|}{N}\right) \sqrt{|C|}(\mu - \epsilon) \geq O\left(\max(\sqrt{\rho}, \sqrt{\log N}) \sqrt{\log N}\right).$$

The proofs of Lemma 4 and Theorem 2 are merged in Appendix B. The main idea is to show that under the null hypothesis, $\mathbf{1}_C^T (\mathbf{y} - \epsilon \mathbf{1}) / \sqrt{|C|}$ is a sub-Gaussian random variable, while under the alternative hypothesis, the maximum likelihood estimator $\mathbf{1}_C^T \mathbf{y} / |C|$ is close to μ with high probability. Similarly to the graph wavelet statistic, (7) shows that the key to detecting the activation is related to the properties of the ground-truth activated node set. When the size of the ground-truth activated node set is larger and the ground-truth activated node set has a small ℓ_1 -norm-based total variation, it is easier for graph scan statistic to detect the activation. Similarly to (5), (7) fails when $|C|$ is too close to N , because the two mean values, $\mathbf{1}_C^T \mathbf{y} / |C|$ and $\mathbf{1}^T \mathbf{y} / N$, in (6) are too close. In other words, $\mathbf{1}^T \mathbf{y} / N$ is a poor estimate for the background noise ϵ . Again, in practice we typically consider $|C| \ll O(N)$, because localized attributes are relatively small compared to the entire graph.

Given the graph scan statistic \hat{g} , the upper bound on the p -value is $2e^{-\frac{\sqrt{2}}{3} \left(\sqrt{\frac{\hat{g}}{8}} - 2 \log 2 - \left(\sqrt{\rho} + \sqrt{\frac{1}{2} \log N} \right) \sqrt{2 \log(N-1)} \right)^2}$. Let our test be level α . We reject the null hypothesis at all $\alpha \geq 2e^{-\frac{\sqrt{2}}{3} \left(\sqrt{\frac{\hat{g}}{8}} - 2 \log 2 - \left(\sqrt{\rho} + \sqrt{\frac{1}{2} \log N} \right) \sqrt{2 \log(N-1)} \right)^2}$. The

threshold is only related to the size of graph N and the cut cost ρ , which is a user-defined parameter.

There are two advantages to the graph scan statistic over the graph wavelet statistic: it is data adaptive and flexible by considering edge weights. Instead of using a pre-constructed graph wavelet basis, graph scan statistic actively searches for the activated node set. Thus, it not only detects whether localized activated node sets exist, but also localizes such regions. It also takes into account edge weights by using the ℓ_1 -norm-based total variation and is more general compared to ℓ_0 -norm-based total variation used in graph wavelet statistic. Note that the ℓ_1 -norm-based total variation and the ℓ_0 -norm-based total variation are the same when we only consider binary edge weights. Thus, all the results based on the ℓ_1 -norm can be directly applied to the ℓ_0 -norm.

Practical algorithms. In the previous analysis, we used the global optimum of \hat{g} in (6); this global optimum is hard to obtain, however, because the optimization problem is combinatorial. We instead consider two practical methods to compute the graph scan statistic: the first obtains a local optimum of the original optimization problem and the second a global optimum of a relaxed optimization problem.

In the first method, we reformulate (6) and solve

$$\hat{g} = \max_t \max_{\mathbf{x}} t \text{KL} \left(\frac{\mathbf{x}^T \mathbf{y}}{t} \parallel \frac{\mathbf{1}^T \mathbf{y}}{N} \right) \quad (8)$$

subject to $\mathbf{x} \in \{0, 1\}^N, \text{TV}_1(\mathbf{x}) \leq \rho, \mathbf{1}^T \mathbf{x} \leq t,$

where \mathbf{x} is an auxiliary attribute to represent $\mathbf{1}_C$ and t denotes $|C|$. Since $\mathbf{1}^T \mathbf{y}/N$ is a small constant, for each t , we optimize over \mathbf{x} to move $\mathbf{x}^T \mathbf{y}/t$ as far away from $\mathbf{1}^T \mathbf{y}/N$ as possible, which is equivalent to maximizing $\mathbf{x}^T \mathbf{y}$ within the feasible region.² Given a fixed t , we solve

$$\mathbf{x}_t^* = \arg \min_{\mathbf{x}} (-\mathbf{x}^T \mathbf{y}), \quad (9)$$

subject to $\mathbf{x} \in \{0, 1\}^N, \text{TV}_1(\mathbf{x}) \leq \rho, \mathbf{1}^T \mathbf{x} \leq t.$

The corresponding Lagrange function is

$$L(\eta_1, \eta_2, \mathbf{x}) = -\mathbf{x}^T \mathbf{y} + \eta_1 (\mathbf{1}^T \mathbf{x} - t) + \eta_2 (\|\Delta \mathbf{x}\|_1 - \rho).$$

The Lagrange dual function is

$$\begin{aligned} Q(\eta_1, \eta_2) &= \min_{\mathbf{x} \in \{0, 1\}^N} L(\eta_1, \eta_2, \mathbf{x}) \\ &= \min_{\mathbf{x} \in \{0, 1\}^N} (-\mathbf{x}^T \mathbf{y} + \eta_1 \mathbf{1}^T \mathbf{x} + \eta_2 \|\Delta \mathbf{x}\|_1) - \eta_1 t - \eta_2 \rho \\ &= q(\eta_1, \eta_2) - \eta_1 t - \eta_2 \rho. \end{aligned}$$

For given η_1, η_2 , the function $q(\eta_1, \eta_2)$ can be efficiently solved by s - t graph cuts [58], [66]. We then maximize $Q(\eta_1, \eta_2)$ by using the simulated annealing and obtain \mathbf{x}_t^* as the optimum of (9). Finally, we optimize over t by evaluating each pair of t and \mathbf{x}_t^* in the objective function (8). Since \mathbf{x} takes only binary values, the optimization problem (9) is not convex. However, previous works show that even the local minimum provides decent results [66] and the computation is remarkably efficient. We call the solution *local graph scan statistic* (LGSS) because it is a local optimum of the original optimization problem (8) by using graph cuts.

²We implicitly assume that $\mathbf{1}_C^T \mathbf{y}/|C| > \mathbf{1}^T \mathbf{y}/N$.

In the second method, we compute the graph scan statistic in a convex fashion by relaxing the original combinatorial optimization problem (8),

$$\hat{r} = \max_t \max_{\mathbf{x}} t \text{KL} \left(\frac{\mathbf{x}^T \mathbf{y}}{t} \parallel \frac{\mathbf{1}^T \mathbf{y}}{N} \right) \quad (10)$$

subject to $\mathbf{x} \in [0, 1]^N, \text{TV}_1(\mathbf{x}) \leq \rho, \mathbf{1}^T \mathbf{x} \leq t.$

The only difference between (8) and (10) is that we relax the feasible set of $\{0, 1\}^N$ to be a convex set $[0, 1]^N$. Given a fixed t , we obtain the optimum \mathbf{x}_t^* by convex programming. We then optimize over t by evaluating each pair of t and \mathbf{x}_t^* in the objective function (10). We call \hat{r} the *convex graph scan statistic* (CGSS). When \hat{r} is larger than some threshold, we detect the activated node set and reject the null hypothesis.

To analyze the convex graph scan statistic, Lemma 5 shows that given a threshold related to the size of the graph N , a user-defined error tolerance δ and cut cost ρ , the type-1 error is upper bounded, Theorem 3 shows that when the attribute strength is sufficiently large, both type-1 and type-2 errors can be upper bounded and Corollary 3 states the condition of the asymptotic distinguishability.

Lemma 5. Let the convex graph scan statistic be \hat{r} in (10). Under the statistical test (3) with $p = 0$, we reject the null hypothesis for all $\hat{r} > \tau$, with

$$\begin{aligned} \tau &= 8 \left(\frac{\log 2N + 1}{\sqrt{(\sqrt{\rho} + \sqrt{\frac{1}{2} \log N})^2 \log N}} + \sqrt{2 \log 2} + \right. \\ &\quad \left. 2 \sqrt{\left(\left(\sqrt{\rho} + \sqrt{\frac{1}{2} \log N} \right)^2 \log N + \sqrt{\frac{9}{2} \log\left(\frac{2}{\delta}\right)} \right)^2} \right). \end{aligned}$$

The corresponding type-1 error is $\mathbb{P}\{T = 1 | H_0^N \text{ is true}\} \leq 1 - (1 - \delta)^2$.

Theorem 3. Let the attribute strength be sufficiently large,

$$\begin{aligned} \left(1 - \frac{|C|}{N}\right) \sqrt{|C|}(\mu - \epsilon) &\geq \left(4\sqrt{\log 2} + 6\sqrt{\log\left(\frac{2}{\delta_1}\right)} + \right. \\ &\quad \frac{2\sqrt{2}(\log 2N + 1)}{\sqrt{(\sqrt{\rho} + \sqrt{\frac{1}{2} \log N})^2 \log N}} + \\ &\quad \left. 4\sqrt{2 \left(\left(\sqrt{\rho} + \sqrt{\frac{1}{2} \log N} \right)^2 \log N + \right.} \right. \\ &\quad \left. \left. \left(\sqrt{\frac{1}{2} + \sqrt{\frac{|C|}{2N}}} \sqrt{\log\left(\frac{2}{\delta_2}\right)} \right) \right) \right). \quad (11) \end{aligned}$$

Then, by using the convex graph scan statistic \hat{r} in Lemma 5, the type-1 error is $\mathbb{P}(T = 1 | H_0^N \text{ is true}) \leq 1 - (1 - \delta_1)^2$ and the type-2 error is $\mathbb{P}(T = 0 | H_1^N \text{ is true}) \leq 1 - (1 - \delta_2)^3$.

We set $\delta_1 = \delta_2 = 1/N$ and obtain the following corollary.

Corollary 3. Using the convex graph scan statistic \hat{r} in (10), H_0^N and H_1^N are asymptotically distinguishable, that is, $\lim_{N \rightarrow \infty} R_N(T) = 0$, when

$$\left(1 - \frac{|C|}{N}\right) \sqrt{|C|}(\mu - \epsilon) \geq O\left(\max(\sqrt{\rho}, \sqrt{\log N})\sqrt{\log N}\right).$$

The proofs of Lemma 5 and Theorem 3 are merged in Appendix C. The main idea is to show that under the null hypothesis, $\mathbf{x}^T(\mathbf{y} - \epsilon\mathbf{1})/\sqrt{\mathbf{1}^T\mathbf{x}}$ is a sub-Gaussian random variable with mean zero, while under the alternative hypothesis, the maximum likelihood estimator $\mathbf{1}_{C|}^T\mathbf{y}/|C|$ is a sub-Gaussian random variable with mean μ . Similarly to the graph wavelet statistic and graph scan statistic, (11) shows that the key to detecting the activation is related to the properties of the ground-truth activated node set.

To compute the convex graph scan statistic, we solve

$$\begin{aligned} \mathbf{x}_t^* &= \arg \min_{\mathbf{x}} -\mathbf{x}^T\mathbf{y}, \\ &\text{subject to } \mathbf{x} \in [0, 1]^N, \text{TV}_1(\mathbf{x}) \leq \rho, \mathbf{1}^T\mathbf{x} \leq t, \end{aligned} \quad (12)$$

for a given t . The objective function is linear and all the constraints are convex, so (12) can be easily solved by a convex optimization solver. Finally, we optimize over t by evaluating each pair of t and \mathbf{x}_t^* in the objective function (10). Because of the convex relaxation, the final solution of \mathbf{x} is not binary and a higher value of x_i indicates a higher confidence that the i th node is activated.

We summarize these two methods for graph scan statistic computation in Algorithm 2. While in practice the convex graph scan statistic outperforms the local graph scan statistic, the local graph scan statistic is more appealing when dealing with large-scale graphs.

Algorithm 2 Graph Scan Statistic

Input \mathbf{y} input attribute
Output \mathbf{x}^* activated local set

Function

For a given t

local graph scan statistic: solve (8) using graph cuts, or

convex graph scan statistic: solve (10) using convex optimization solver

search over t , return the largest t $\text{KL}\left(\frac{\mathbf{x}_t^*{}^T\mathbf{y}}{t} \parallel \frac{\mathbf{1}^T\mathbf{y}}{N}\right)$ and \mathbf{x}_t^* as \mathbf{x}^*

C. Discussion

We now compare the proposed statistics.

- The graph wavelet statistic selects a feature by projecting given attributes onto a pre-constructed graph wavelet basis and is a data-independent and discriminative approach, which works only for detection.³ The graph scan statistic searches over graphs and localizes the localized attribute and is a data-dependent and generative approach, which works for both detection and localization.
- From a statistical perspective, the graph wavelet statistic requires that the attribute strength $\sqrt{|C|}(\mu - \epsilon)$ be larger than $O(\rho \log^2 N)$ as in Theorem 1 while the graph scan statistic requires that the attribute strength $(1 - |C|/N)\sqrt{|C|}(\mu - \epsilon)$ be larger than $O(\max(\rho, \log N) \log N)$ as in Theorems 2 and 3. Appendix D shows that the proposed graph statistics significantly outperforms a naive approach, which uses the mean value as statistic.

³It is possible to use the graph wavelet basis and nonlinear approximation to localize the localized attribute; this is beyond the scope of this paper.

- From a computational perspective, the graph wavelet statistic is the cheapest to compute. The graph scan statistic implemented through the local graph scan statistic is also efficient by using efficient graph cuts, while the convex graph scan statistic costs the most because it needs to solve a series of convex optimization problems.
- From the perspective of empirical performance, the convex graph scan statistic typically provides the best performance followed by the graph wavelet statistic. Because graph cuts only provide a local solution, computing the local graph scan statistic is sensitive to the choice of parameters and initial conditions.

V. EXPERIMENTAL RESULTS

We now evaluate our proposed methods on three datasets. We study how detection performance changes according to parameters on a simulated dataset. We observe that the size of the ground-truth activated node set is crucial for the detection, which is consistent with Theorems 1, 2 and 3. We validate the effectiveness of our proposed methods on two real-world problems: air-pollution detection and attribute ranking for community detection.

A. Simulation Results

We generate simulated data on the Minnesota road graph [67] and study how the parameters, including the activation probability inside the localized pattern μ , the noise level ϵ and the activation size $|C|$, influence the detection performance. The Minnesota road graph is a standard dataset including 2642 nodes and 3304 undirected edges [67]. We generate two binary graph signals as follows: we randomly choose one node as a cluster head and assign all other nodes that are within k steps to the cluster head to an activated node set, where k varies from 6 to 12. Figures 3 (a) and (b) show these two binary graph signals, where the nodes in yellow indicates the activated nodes and the nodes in blue indicates the nonactivated nodes. Using these two binary graph signals as templates, we then generate two classes of random graph signals: for attributes under H_1^N , each node inside the activated region is activated with probability μ and each node outside the activated region is activated with probability ϵ . Both μ and ϵ vary from 0.05 to 0.95 with interval of 0.1. For each combination of μ and ϵ , we generate corresponding attributes under H_0^N , the activation probability for each node is $(\mu|C| + \epsilon(N - |C|))/N$. We run 100 random tests to compute the statistics and quantify the performance by the area under the receiver operating characteristic curve (AUC) [63].

Figures 3 (c), (e) and (g) show AUCs of the graph wavelet statistic, the local graph scan statistic (LGSS) and the convex graph scan statistic (CGSS) for the small activated region, where the step $k = 6$. For example, each block in Figure 3 (c) corresponds to the AUC of the graph wavelet statistic given a pair of μ and ϵ . A whiter block indicates a higher AUC and a better performance. Note that when μ is smaller than ϵ , we did not run the experiments and directly set the corresponding AUC to zero. We see that the graph wavelet statistic has a similar performance with the convex graph scan statistic and

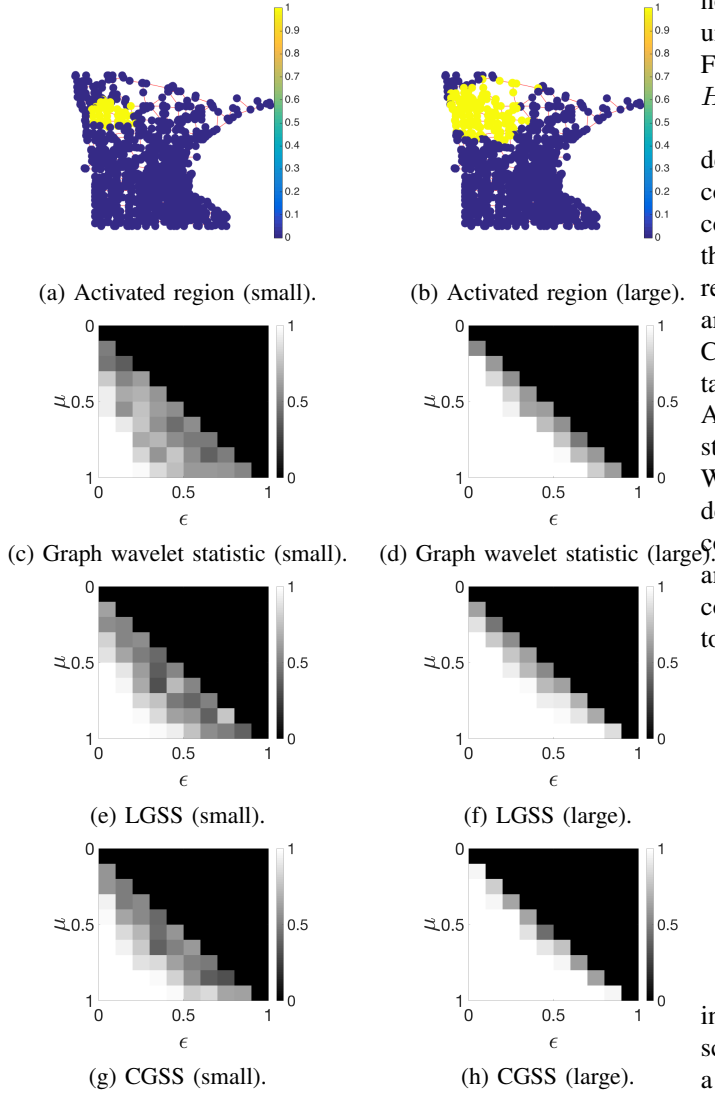


Fig. 3: Comparison of graph wavelet statistic and graph scan statistic on the simulated dataset. The left column shows the results for a small activated region and the right column shows the results for a large activated region. All methods perform better when an activated region is larger. For a same activated region, all methods perform better when $\mu - \epsilon$ is larger.

both outperform the local graph scan statistic. Figures 3 (d), (f) and (h) show AUCs of the graph wavelet statistic, the local graph scan statistic and the convex graph scan statistic for the large activated region, where the step $k = 12$. We see that the convex graph scan statistic perform the best and the graph wavelet statistic has a slightly better performance than the local graph scan statistic. Comparing the results from two activated regions (left column versus right column in Figure 3), we see that all the methods perform better when the activated region is large. For example, both Figures 3 (c) and (d) use graph wavelet statistic. Given a fixed pair of μ and ϵ , a large activated region has a larger AUC, indicating higher probability to be detection.

To have a clearer understanding of how the proposed statistics work, we set the activation probability $\mu = 0.35$ and the

noise level $\epsilon = 0.15$. Figures 4 (b) and (c) show the attribute under H_1^N and H_0^N given the ground-truth activated region in Figure 4 (a). When we compare the attributes under H_1^N and H_0^N , it is clear that distinguishing H_1^N from H_0^N is not trivial.

Figures 4 (d), (f) and (h) compare the activated regions detected by graph wavelet basis, local graph scan statistic and convex graph scan statistic under H_1^N . The graph wavelet basis compares the average values between the nodes in yellow and the nodes in blue. When the difference is large, the activated region is detected. Ideally, we want all the nodes in blue are activated and all the nodes in yellow are nonactivated. Considering the graph wavelet basis is designed before obtaining any data, it captures the activated region fairly well. As expected, local graph scan statistic and convex graph scan statistic perform similarly and capture the activated region well. We also show the noisy attribute and the activated regions detected by graph wavelet basis, local graph scan statistic and convex graph scan statistic under H_0^N in Figures 4 (c), (e), (g) and (i). The graph wavelet basis, local graph scan statistic and convex graph scan statistic cannot detect regions that are close to the true activated region from the pure noisy attribute.

	Attribute under H_0^N Figure 4 (b)	Attribute under H_1^N Figure 4 (c)
Activated nodes	422	420
Modularity	9.1228	1.1422
Cut cost	845	887
Wavelet	1.50	2.14
LGSS	57.58	68.12
CGSS	42.97	72.33

TABLE I: Facts about the data in Figures 4 (b) and (c).

Table I shows some facts about data in Figures 4 (b) and (c), including modularity, cut cost, graph wavelet statistic, graph scan statistic and convex graph scan statistic. Modularity is a popular metric to measure the strength of communities [2]. Networks with high modularity have dense connections within communities but sparse connections in different communities. Mathematically, the modularity of a binary attribute $\mathbf{1}_C \in \mathbb{R}^N$ is⁴

$$\text{Modularity} = \sum_{i,j} \left(A_{i,j} - \frac{d_i d_j}{M} \right) (\mathbf{1}_C)_i (\mathbf{1}_C)_j,$$

where d_i is the degree of the i th node, $M = \sum_i d_i$ is the total number of edges, and $(\mathbf{1}_C)_i = 1$ when the i th node is activated; otherwise, $(\mathbf{1}_C)_i = 0$. A large modularity means the activated nodes are strongly connected.

Graph cuts measure the cost to separate a community from the other nodes. Mathematically, the cut cost of the binary attribute $\mathbf{1}_C \in \mathbb{R}^N$ is $\text{Cut} = \text{TV}_0(\mathbf{1}_C)$. A small cut cost means the activated nodes are easily separated from the nonactivated nodes.

We expect that under H_1^N , modularity is larger, indicating dense internal connections, and the cut cost is smaller, indicating few external connections. From Table I, however, we see that attributes under H_0^N and H_1^N contain similar number of activated nodes, the modularity under H_1^N is smaller than the modularity under H_0^N , indicating the activated nodes under

⁴We drop a constant factor M here.

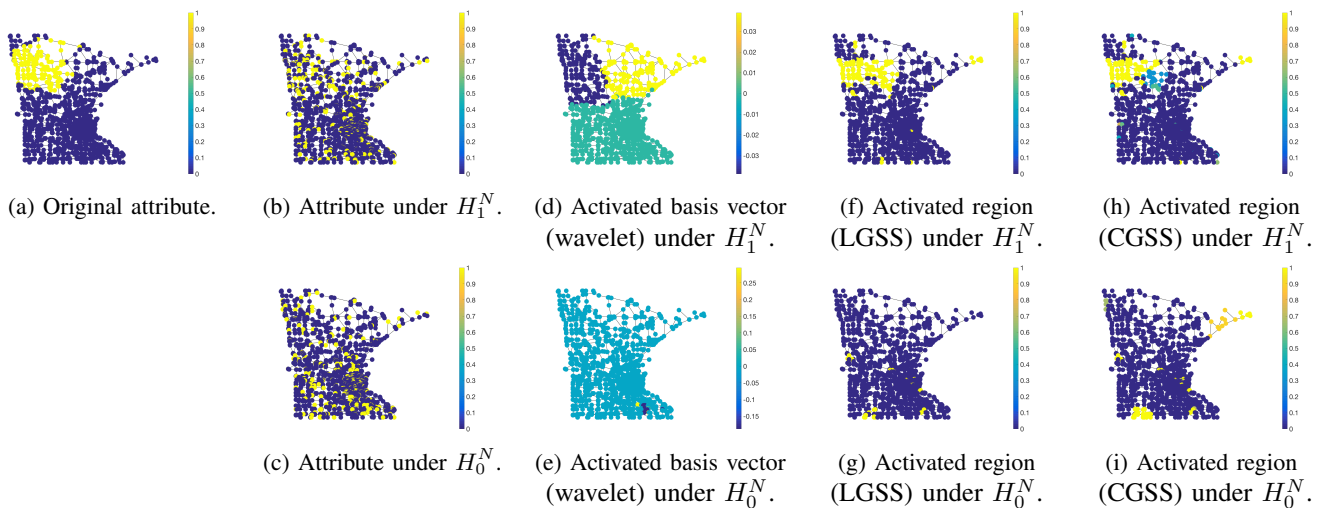


Fig. 4: Illustration of how the proposed statistics work. Under H_1^N , the graph wavelet statistic, local graph scan statistic and convex graph scan statistic denoise the given attribute and localize the true community. Under H_0^N , the graph wavelet basis, local graph scan statistic and convex graph scan statistic cannot localize the true community. The denoising procedure is the key to robustness. Graph wavelet statistic extracts features from original attributes and is a discriminative approach. (d) shows a graph wavelet basis vector corresponding to the maximum absolute value of the graph wavelet coefficients. Graph scan statistic recovers denoised attributes and is a generative approach. (f) and (h) show the activated regions recovered by graph scan statistics. For CGSS, due to the convex relaxation, the recovered activated region is not binary. A higher value of x_i indicates a higher confidence that the i th node is activated.

H_0 have even stronger internal connections. The cut cost under H_0^N is smaller than the cut cost under H_1^N , indicating the activated nodes under H_0^N are easier to be separated from the nonactivated nodes. It is clear that both modularity and number of cuts fail when the noise level is high. On the other hand, the graph wavelet statistic, local graph scan statistic and convex graph scan statistic under H_1^N are much higher than those under H_0^N , indicating these three proposed statistics succeed even when the noise level is high. Graph wavelet statistic is robust because it selects a useful feature by using the graph wavelet basis. The graph scan statistic also is robust is because it localizes the true activated region first, which is equivalent to denoise the attribute based on the graph structure. Based on the denoised attribute, we compute the statistic values and the results are more robust. In other words, graph wavelet statistic extracts features from original attributes and is a discriminative approach to detect and graph scan statistic recovers a denoised attributes and is a generative approach.

In terms of the computational complexity, for each random test, it takes around 30 seconds to construct the graph wavelet basis, around 0.01 seconds to calculate the graph wavelet statistic, around 5 seconds to calculate the local graph scan statistic, around 10 seconds to calculate the convex graph scan statistic. Overall, the proposed statistics provide efficient and effective performances.

B. High Air-Pollution Detection

The first real-world example is on air-pollution detection; we are interested in particle pollution as indicated by the fine particulate matter (PM 2.5), particles that are 2.5 micrometers in diameter or smaller and can only be seen with an electron microscope. These tiny particles are produced from all types of

combustion, including motor vehicles, power plants, residential wood burning, forest fires, agricultural burning, and some industrial processes. High PM 2.5 is linked to increased mortality rate for patients suffering from heart and lung disease [68]. We aim to provide an efficient and effective approach for detecting high PM 2.5 regions, which can guide authorities in designing remedial measures.

The dataset comes from [69] and includes 756 operating sensors that record the daily average at various locations; Figure 5(a) shows the PM 2.5 distribution on July 1st, 2014, in the mainland U.S. We construct a ten-nearest neighbor graph with each sensor a node connecting to ten neighboring sensors. Figure 5(b) shows the input attribute obtained by thresholding the measurements above 15 (high-pollution cities, marked in yellow).

When high-pollution cities are far from each other, high pollution may be caused by random events or measurement failures, which makes the detection sensitive to noise. When high-pollution cities are clustered together, high pollution is prevalent in the area, which makes the detection robust. Using detection algorithms here aims to answer whether high-pollution cities are clustered and provides a more robust high-pollution detector. In Figure 5(b), high-pollution cities seem to concentrate in the mid-east part of the U.S. We now verify whether this claim is true by using the graph wavelet statistic, graph scan statistic and convex graph scan statistica. To make a comparison, we also simulate 1,000 attributes (graph signals) that have the same number of high-pollution cities, but are scattered across the U.S. Figures 5(e)–(g) show the values of the graph statistics. For each plot, the red dashed line shows the value of the graph statistic for the real pollution attribute as shown in Figure 5(b) and the black curves show the empirical

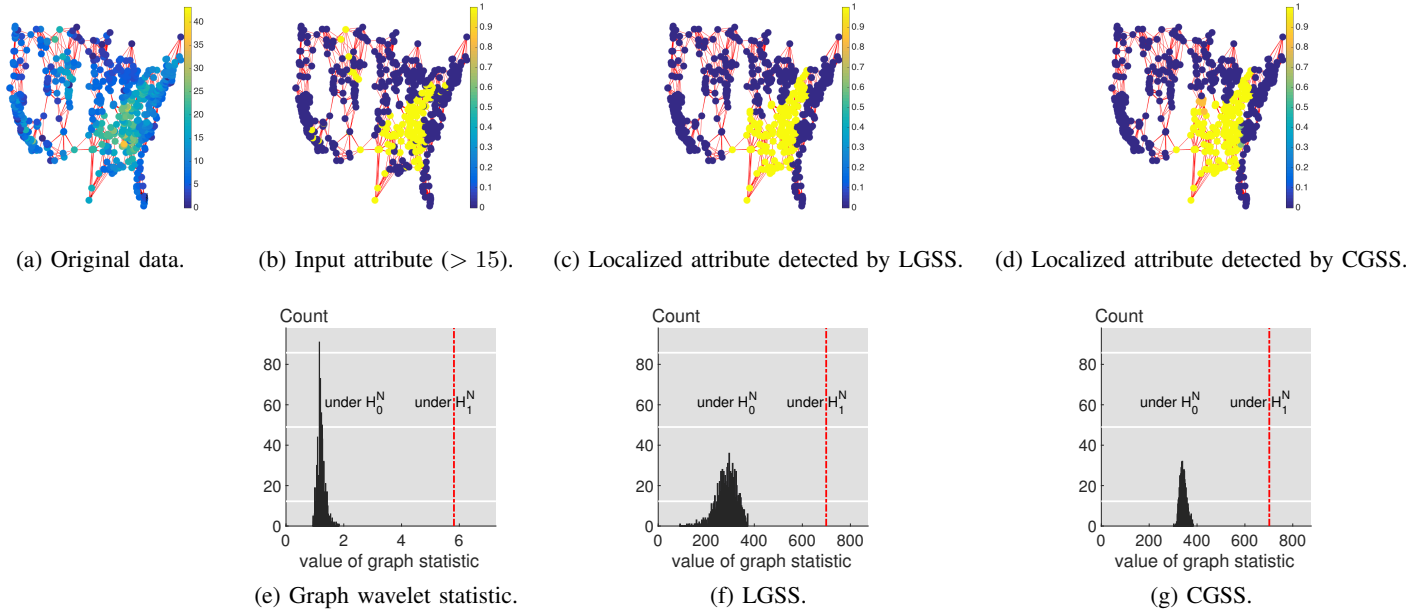


Fig. 5: Detecting the high-pollution region on July 1st, 2014. (a) Original data. (b) High-pollution cities (in yellow). (c)–(d) High-pollution regions recovered by the graph scan statistics. (e)–(g) Detection of high-pollution regions from random attributes. For each plot, the red dashed line shows the value of the graph statistic for the real pollution graph signal from (b) and the black curves show the empirical histograms of the graph statistics under 1,000 random trials.

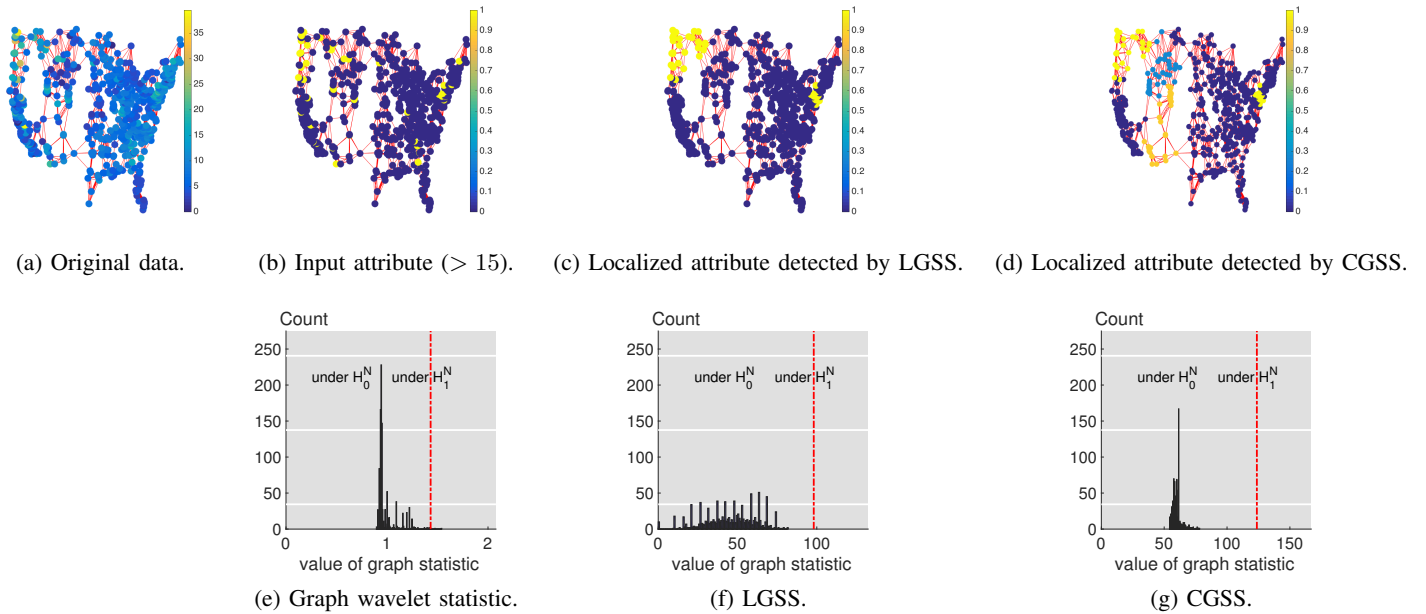


Fig. 6: Detecting the high-pollution region on December 1st, 2014. (a) Original data. (b) High-pollution cities (in yellow). (c)–(d) High-pollution regions recovered by the graph scan statistics. (e)–(g) Detection of high-pollution regions from random attributes. For each plot, the red dashed line shows the value of the graph statistic for the real pollution graph signal from (b) and the black curves show the empirical histograms of the graph statistics under 1,000 random trials.

histograms of the graph statistics under 1,000 random trials. We see that the values of the graph statistics of the real attributes are always much larger than those of the scattered simulated attributes for all three statistics, which means that it is easy to reject the null hypothesis and confirm that the high-pollution cities in Figure 5(b) form a local cluster. Figures 5(c)–(d) show the localized attributes detected by the graph scan statistic and the convex graph scan statistic, respectively. We see that these two detected localized attributes are similar and confirm that the mideast region has relatively high pollution.

We did the same experiments for the data collected on December 1st, 2014, as shown in Figure 6(a). The dataset includes 837 operating sensors (the operating sensors are different every day) and we still construct a ten-nearest neighbor graph. We see that high-pollution cities are more scattered, though some of them seem to cluster in the northwestern corner. Figures 6(e)–(g) show that the values of the graph statistics of the real attributes are still larger than those of the scattered simulated attributes for all three statistics most of the time, which confirms that high-pollution cities cluster together. Again, the two detected localized attributes in Figures 6(c)–(d) confirm that the northwestern corner has relatively high pollution.

C. Ranking Attributes for Community Detection

As discussed in Section III, while relevant node attributes improve the accuracy of community detection and add meaning to the detected communities, irrelevant attributes may harm the accuracy and cause computational inefficiency. By using the proposed statistics, we can quantify the usefulness of each attribute. As localized attributes tend to be related to community structure, our methods can serve to filter out the most useful attributes for community detection.

As a dataset, we use the IEEE Xplore database to find working collaborators [70]. We construct three bipartite networks: papers and journals, papers and authors and papers and keywords (keywords are automatically assigned by IEEE). We focus on papers in ten journals: IEEE Transactions on Magnetics, Information Theory, Nuclear Science, Signal Processing, Electron Devices, Communications, Applied Superconductivity, Automatic Control, Microwave Theory and Techniques and Antennas and Propagation.

We project the bipartite network of papers and authors onto authors to create a co-authorship network where two authors are connected when they co-author at least four papers. We keep the largest connected component of the co-authorship network. As explained in more detail below, we project the network of papers and journals and the network of papers and authors onto the authors in the largest connected component to create the author-journal matrix, where rows denote authors and columns denote journals. We project the network of papers and keywords and a network of papers and authors onto the authors in the largest connected component to create the author-keyword matrix, where rows denote authors and columns denote keywords.

The entire dataset includes the co-authorship network with 7,330 authors (nodes) and 108,719 co-authorships (edges),

the author-journal matrix with ten journals and the author-keyword matrix with 3,596 keywords (attributes). We want to detect academic communities (defined based on the journal) based on the graph structure and attributes. Since our attributes are keywords, we use those to improve community detection; for example, in the signal processing community, some frequently-used keywords are ‘filtering’, ‘Fourier transform’ and ‘wavelets’. Our ground truth communities are the ten journals; when authors publish at least ten papers in the same journal, we assign them to an eponymous community.

The goal is to rank all keywords based on their contribution to community detection, where the value of the corresponding statistic is used to determine the rank. We consider four ranking methods: graph wavelet statistic based ranking, local graph scan statistic based ranking, modularity-based ranking [2] and cut-based ranking [59]. We did not use the convex graph scan statistic due to computational cost. For the first two ranking methods, we compute the values of the graph statistics and rank the keywords according to the values of the graph statistics in a descending order. This is because a larger statistic means a larger probability that this keyword forms a community. For the modularity-based ranking, we compute the modularity of each keyword and rank the keywords according to modularity in a descending order. For the cut-based ranking, we compute the cut cost of each keyword and rank the keywords according to the cut cost in a ascending order. Table II lists the top ten most important keywords that potentially form communities provided by the above four rankings.

To quantify the real community detection power of keywords, we compare each keyword to the ground-truth community and compute the correspondence by using the average F1 score [60], [46]. Let C^* be a set of the ground-truth communities and \hat{C} a set of the activated node sets provided by the node attributes. Each node set $\hat{C}_i \in \hat{C}$ collects the nodes that have the same attribute. The average F1 score is

$$\frac{1}{2|C^*|} \sum_{C_i \in C^*} \text{F1}(C_i, \hat{C}_{g(i)}) + \frac{1}{2|\hat{C}|} \sum_{\hat{C}_i \in \hat{C}} \text{F1}(\hat{C}_{g'(i)}, \hat{C}_i),$$

where the best matching g and g' are

$$g(i) = \arg \max_j \text{F1}(C_i, \hat{C}_j) \text{ and } g'(i) = \arg \max_j \text{F1}(C_j, \hat{C}_i),$$

where $\text{F1}(C_i, \hat{C}_j)$ is the harmonic mean of precision and recall. A large average F1 score means that the community induced by a keyword agrees with the community induced by journal papers. We also compute the average F1 score of each keyword and rank the keywords according to the average F1 scores in a descending order, which is the ground-truth ranking. We compare the four estimated rankings with the ground-truth ranking by using the Spearman’s rank correlation coefficient [71]. The Spearman correlation coefficient is defined as the Pearson correlation coefficient between the ranked variables,

$$\text{correlation} = 1 - \frac{6 \sum |p_i - q_i|^2}{N(N^2 - 1)},$$

where $p_i - q_i$ is the difference between two rankings. The Spearman correlation coefficients of modularity-based ranking, cut-based ranking, graph wavelet statistic based ranking and local

Modularity-based ranking	Cut-based ranking	Graph wavelet statistic based ranking	Local graph scan statistic based ranking
Dielectrics	Data analysis	Subtraction techniques	Maximum likelihood detection
Next generation networking	Parasitic capacitance	Mice	Upper bound
Undulators	Alpha particles	Parallel architectures	Antenna arrays
Pathology	Strips	Integrated circuit interconnections	Biological information theory
Servosystems	Customer relationship management	Yttrium barium copper oxide	Interchannel interference
Electronic design automation	Biology computing	Dielectrics	Microscopy
Subtraction techniques	Uncertainty	Distributed Bragg reflectors	Signal analysis
Optical noise	Piecewise linear techniques	Fuel economy	Broadcasting
Implants	Forensics	Magnetic analysis	Array signal processing
Biomedical signal processing	Oceans	Tactile sensors	Time-varying systems

TABLE II: Top ten most important keywords that potentially form academic communities.

graph scan statistic based ranking are shown in Figure 7. We see that the graph wavelet statistic and local graph scan statistic outperform other methods. Cut-based ranking performs poorly because it may rank infrequent keywords higher. To account for this effect, we also consider the average modularity—the modularity divided by the number of activated authors and the average cut cost—the cut cost divided by the number of activated authors. We see that the average cut cost performs much better than the total cuts.

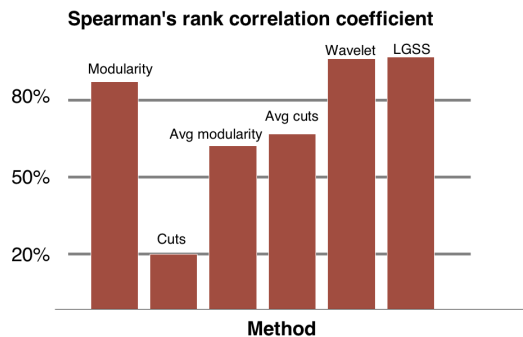


Fig. 7: Comparison of Spearman's rank correlation coefficients; the higher the correlation coefficient, the higher correlation to the ground-truth ranking.

Figure 8 compares the average F1 scores as a function of individual keywords ordered by the six ranking methods. The x -axis is the ranking provided by the proposed ranking methods and the y -axis is the average F1 score of the corresponding keyword. For example, since the local graph scan statistic ranks *Maximum likelihood detection* first, we put the corresponding average F1 score as the first element on the red curve (leftmost). We expect that the curve goes down as the rank increases because a good ranking method ranks the important keywords higher. We also use cluster affiliation model for big networks (BIGCLAM, shown in black), a large-scale overlapping community detection algorithm to provide a baseline [60]. We see that the local graph scan statistic is slightly better than the graph wavelet statistic and both of them outperform the other methods, which is consistent with the results given by the Spearman correlation coefficients in Figure 7. Average cuts rank important keywords lower, causing the F1 score to increase as the rank decreases. The average cuts fail because small average cuts may come from just a few activations. For example, a keyword activating only one author has a small cut number, although this keyword is actually

trivial. Surprisingly, using high-ranking keywords selected by LGSS and wavelets works even better than BIGCLAM on the task of community detection. The reason may be that in this co-authorship network, only some keywords are informative and strongly related to the journals, which are the ground-truth communities, while most keywords may provide trivial or misleading information.

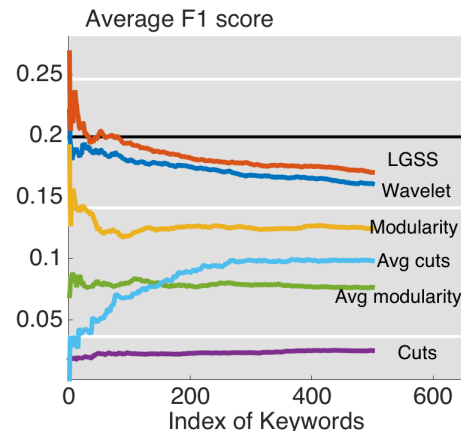


Fig. 8: Comparison of the average F1 score as a function of the top k ranked keywords; the higher the average F1 score, the higher the detection performance by using each individual keyword. The black horizontal line shows the performance of BIGCLAM, a large-scale overlapping community detection algorithm.

VI. CONCLUSIONS

The goal of this paper was to detect localized attributes on a graph when observations are corrupted by noise. We formulate hypothesis tests to decide whether the observations activate a community in a graph corrupted by Bernoulli noise. We model our noisy attributes as binary graph signals: a positive signal coefficient indicates an activated node; when the activated nodes form a cluster, we say that the attribute contains a localized activation. We proposed two statistics for testing: graph wavelet statistic and graph scan statistic, both of which are shown to be efficient and statistically effective to detect activations. The graph wavelet statistic works by detecting the boundary of the underlying localized attribute while the graph scan statistic works by localizing the underlying localized attribute, which is equivalent to denoising a given attribute.

Theorems 1, 2 and 3 show that the key to distinguishing the activation is the activation probability difference and the size of the activated region. We validate the effectiveness and robustness of the proposed methods on simulated data first; experimental results match the theorems well. We further validate them on two real-world applications: high air-pollution detection and attribute ranking; experimental results show the proposed statistics are effective and efficient.

REFERENCES

- [1] M. Jackson, *Social and Economic Networks*, Princeton University Press, 2008.
- [2] M. Newman, *Networks: An Introduction*, Oxford University Press, 2010.
- [3] S. Chen, R. Varma, A. Singh, and J. Kovačević, "Signal recovery on graphs: Fundamental limits of sampling strategies," *IEEE Trans. Signal and Inform. Process. over Networks*, vol. 2, no. 4, pp. 1–16, Dec. 2016.
- [4] M. Girvan and M. E. J. Newman, "Community structure in social and biological networks," *Proc. Nat. Acad. Sci.*, vol. 99, pp. 7821–7826, 2002.
- [5] S. Brin and L. Page, "The anatomy of a large-scale hypertextual web search engine," *Comput. Netw. ISDN Syst.*, vol. 30, no. 1-7, pp. 107–117, Apr. 1998.
- [6] M. Xie, S. Han, B. Tian, and S. Parvin, "Anomaly detection in wireless sensor networks: A survey," *J. Netw. Comput. Appl.*, vol. 34, no. 4, pp. 1302–1325, July 2011.
- [7] D. I. Shuman, S. K. Narang, P. Frossard, A. Ortega, and P. Vandergheynst, "The emerging field of signal processing on graphs: Extending high-dimensional data analysis to networks and other irregular domains," *IEEE Signal Process. Mag.*, vol. 30, pp. 83–98, May 2013.
- [8] A. Sandryhaila and J. M. F. Moura, "Discrete signal processing on graphs," *IEEE Trans. Signal Process.*, vol. 61, no. 7, pp. 1644–1656, Apr. 2013.
- [9] S. Chen, R. Varma, A. Sandryhaila, and J. Kovačević, "Discrete signal processing on graphs: Sampling theory," *IEEE Trans. Signal Process.*, vol. 63, no. 24, pp. 6510–6523, Dec. 2015.
- [10] A. Anis, A. Gadde, and A. Ortega, "Efficient sampling set selection for bandlimited graph signals using graph spectral proxies," *IEEE Trans. Signal Process.*, vol. 64, no. 14, pp. 3775–3789, July 2015.
- [11] X. Wang, P. Liu, and Y. Gu, "Local-set-based graph signal reconstruction," *IEEE Trans. Signal Process.*, vol. 63, no. 9, May 2015.
- [12] A. G. Marques, S. Segarra, G. Leus, and A. Ribeiro, "Sampling of graph signals with successive local aggregations," *IEEE Trans. Signal Process.*, Dec 2015.
- [13] S. K. Narang, Akshay Gadde, and Antonio Ortega, "Signal processing techniques for interpolation in graph structured data," in *Proc. IEEE Int. Conf. Acoust., Speech, Signal Process.*, Vancouver, May 2013, pp. 5445–5449.
- [14] S. Chen, A. Sandryhaila, J. M. F. Moura, and J. Kovačević, "Signal recovery on graphs: Variation minimization," *IEEE Trans. Signal Process.*, vol. 63, no. 17, pp. 4609–4624, Sept. 2015.
- [15] D. Romero, M. Ma, and G. B. Giannakis, "Kernel-based reconstruction of graph signals," *arXiv preprint arXiv:1605.07174*, 2016.
- [16] M. S. Kotzagiannidis and P. L. Dragotti, "Sampling and reconstruction of sparse signals on circulant graphs—an introduction to graph-FRI," *arXiv preprint arXiv:1606.08085*, 2016.
- [17] X. Zhu and M. Rabbat, "Approximating signals supported on graphs," in *Proc. IEEE Int. Conf. Acoust., Speech, Signal Process.*, Kyoto, Mar. 2012, pp. 3921–3924.
- [18] S. Chen, R. Varma, A. Singh, and J. Kovačević, "Signal representations on graphs: Tools and applications," *arXiv:1512.05406 [cs.AI]*, Dec. 2015.
- [19] A. Agaskar and Y. M. Lu, "A spectral graph uncertainty principle," *IEEE Trans. Inf. Theory*, vol. 59, no. 7, pp. 4338–4356, July 2013.
- [20] M. Tsitsvero, S. Barbarossa, and P. D. Lorenzo, "Signals on graphs: Uncertainty principle and sampling," *IEEE Trans. Signal Process.*, vol. 64, pp. 4845–4860, Sept. 2016.
- [21] N. Perraudin and P. Vandergheynst, "Stationary signal processing on graphs," *arXiv preprint arXiv:1603.04667*, Jan. 2016.
- [22] A. G. Marques, S. Segarra, G. Leus, and A. Ribeiro, "Stationary graph processes and spectral estimation," *arXiv preprint arXiv:1603.04667*, Mar. 2016.
- [23] D. Thanou, D. I. Shuman, and P. Frossard, "Learning parametric dictionaries for signals on graphs," *IEEE Trans. Signal Process.*, vol. 62, pp. 3849–3862, June 2014.
- [24] S. K. Narang and A. Ortega, "Perfect reconstruction two-channel wavelet filter banks for graph structured data," *IEEE Trans. Signal Process.*, vol. 60, pp. 2786–2799, June 2012.
- [25] S. K. Narang and Antonio Ortega, "Compact support biorthogonal wavelet filterbanks for arbitrary undirected graphs," *IEEE Trans. Signal Process.*, vol. 61, no. 19, pp. 4673–4685, Oct. 2013.
- [26] V. N. Ekambaram, G. C. Fanti, B. Ayazifar, and K. Ramchandran, "Spline-like wavelet filterbanks for multiresolution analysis of graph-structured data," *IEEE Trans. Signal and Information Processing over Networks*, vol. 1, no. 4, pp. 268–278, 2015.
- [27] J. Zeng, G. Cheung, and A. Ortega, "Bipartite subgraph decomposition for critically sampled wavelet filterbanks on arbitrary graphs," in *Proc. IEEE Int. Conf. Acoust., Speech, Signal Process.*, Shanghai, Mar. 2016, pp. 6210–6214.
- [28] S. Chen, A. Sandryhaila, J. M. F. Moura, and J. Kovačević, "Signal denoising on graphs via graph filtering," in *Proc. IEEE Glob. Conf. Signal Information Process.*, Atlanta, GA, Dec. 2014, pp. 872–876.
- [29] N. Tremblay and P. Borgnat, "Graph wavelets for multiscale community mining," *IEEE Trans. Signal Process.*, vol. 62, pp. 5227–5239, Oct. 2014.
- [30] X. Dong, P. Frossard, P. Vandergheynst, and N. Nefedov, "Clustering on multi-layer graphs via subspace analysis on Grassmann manifolds," *IEEE Trans. Signal Process.*, vol. 62, no. 4, pp. 905–918, Feb. 2014.
- [31] P.-Y. Chen and A.O. Hero, "Local Fiedler vector centrality for detection of deep and overlapping communities in networks," in *Proc. IEEE Int. Conf. Acoust., Speech, Signal Process.*, Florence, 2014, pp. 1120–1124.
- [32] S. Kar and J. M. F. Moura, "Distributed consensus algorithms in sensor networks with imperfect communication: Link failures and channel noise," *IEEE Trans. Signal Process.*, vol. 57, no. 1, pp. 355–369, 2009.
- [33] J. Du, S. Ma, Y.-C. Wu, and H. V. Poor, "Distributed hybrid power state estimation under PMU sampling phase errors," *IEEE Trans. Signal Process.*, vol. 62, no. 16, pp. 4052–4063, 2014.
- [34] D. K. Hammond, P. Vandergheynst, and R. Gribonval, "Wavelets on graphs via spectral graph theory," *Appl. Comput. Harmon. Anal.*, vol. 30, pp. 129–150, Mar. 2011.
- [35] S. K. Narang, G. Shen, and A. Ortega, "Unidirectional graph-based wavelet transforms for efficient data gathering in sensor networks," in *Proc. IEEE Int. Conf. Acoust., Speech, Signal Process.*, Dallas, TX, Mar. 2010, pp. 2902–2905.
- [36] D. I. Shuman, M. J. Faraji, and P. Vandergheynst, "A multiscale pyramid transform for graph signals," *IEEE Trans. Signal Process.*, vol. 64, pp. 2119–2134, Apr. 2016.
- [37] L. Akoglu, H. Tong, and D. Koutra, "Graph based anomaly detection and description: A survey," *Data Min. Knowl. Discov.*, vol. 29, no. 3, pp. 626–688, May 2015.
- [38] Y. Y. Ahn, J. P. Bagrow, and S. Lehmann, "Link communities reveal multiscale complexity in networks," *Nature*, vol. 7307, pp. 7821–7826, Aug. 2010.
- [39] E. Abbe, A. S. Bandeira, and G. Hall, "Exact recovery in the stochastic block model," *IEEE Trans. Inf. Theory*, vol. 62, no. 1, pp. 471–487, 2016.
- [40] S. Fortunato, "Community detection in graphs," *Physics Reports*, vol. 486, pp. 75–174, Feb. 2010.
- [41] J. Sharpnack, A. Rinaldo, and A. Singh, "Sparsistency of the edge lasso over graphs," in *Proc. Int. Conf. Artif. Intell. and Stat.*, La Palma, Apr. 2012, pp. 1028–1036.
- [42] Y.-X. Wang, J. Sharpnack, A. Smola, and R. J. Tibshirani, "Trend filtering on graphs," in *Proc. Int. Conf. Artif. Intell. and Stat.*, San Diego, CA, May 2015.
- [43] E. Arias-Castro, E. J. Candès, and A. Durand, "Detection of an anomalous cluster in a network," *Ann. Stat.*, vol. 39, no. 1, pp. 278–304, 2011.
- [44] J. Sharpnack, A. Rinaldo, and A. Singh, "Change-point detection over graphs with the spectral scan statistic," in *Proc. Artif. Intell. and Stat.*, 2013.
- [45] J. Sharpnack, A. Krishnamurthy, and A. Singh, "Near-optimal anomaly detection in graphs using Lovasz extended scan statistic," in *Proc. Neural Information Process. Syst.*, 2013.
- [46] J. Yang, J. J. McAuley, and J. Leskovec, "Community detection in networks with node attributes," in *Proc. IEEE Int. Conf. Data Mining*, Dallas, TX, Dec. 2013, pp. 1151–1156.
- [47] M. Vetterli, J. Kovačević, and V. K. Goyal, *Foundations of Signal Processing*, Cambridge University Press, Cambridge, 2014, <http://foundationsofsignalprocessing.org>.
- [48] D. O. North, "An analysis of the factors which determine signal/noise discrimination in pulsed-carrier systems," *Proc. IEEE*, vol. 51, pp. 1016–1027, July 1963.

- [49] R. C. Gonzalez and R. E. Woods, *Digital Image Processing*, Prentice Hall, Englewood Cliffs, NJ, 2002.
- [50] A. Mahalanobis, B. V. K. V. Kumar, and D. Casasent, "Minimum average correlation energy filters," *Appl. Opt.*, vol. 26, pp. 3633–3640, 1987.
- [51] J. D. Haupt, R. M. Castro, and R. D. Nowak, "Distilled sensing: selective sampling for sparse signal recovery," in *Proc. Int. Conf. Artif. Intell. and Stat.*, Clearwater Beach, FL, Apr. 2009, pp. 216–223.
- [52] V. Cevher, P. Indyk, C. Hegde, and R. G. Baraniuk, "Recovery of clustered sparse signals from compressive measurements," in *Proc. Sampling Theory Appl.*, Marseille, May 2009.
- [53] S. Zou, Y. Liang, and V. H. Poor, "Nonparametric detection of an anomalous disk over a two-dimensional lattice network," in *Proc. IEEE Int. Conf. Acoust., Speech, Signal Process.*, Shanghai, 2016, pp. 2394–2398.
- [54] C. Hu, L. Cheng, J. Sepulcre, G. E. Fakhri, Y. M. Lu, and Q. Li, "Matched signal detection on graphs: Theory and application to brain network classification," in *Proc. Int. Conf. Inf. Process. Med. Imaging*, Pacific Grove, CA, 2013.
- [55] A. Krishnamurthy, "Minimaxity in structured normal means inference," <http://arxiv.org/pdf/1506.07902>, 2015.
- [56] J. Heydari, A. Tajer, and H. V. Poor, "Quickest detection of Gaussian Markov random field," in *Annual Allerton Conference on Communication, Control, and Computing*, Monticello, IL, Sept. 2015, pp. 808–814.
- [57] J. Sharpnack, A. Krishnamurthy, and A. Singh, "Detecting activations over graphs using spanning tree wavelet bases," in *Proc. Int. Conf. Artif. Intell. and Stat.*, Scottsdale, AZ, Apr. 2013.
- [58] Y. Boykov, O. Veksler, and R. Zabih, "Fast approximate energy minimization via graph cuts," *IEEE Trans. Pattern Anal. Mach. Intell.*, vol. 20, no. 11, pp. 1222–1239, Nov. 2001.
- [59] U. V. Luxburg, "A tutorial on spectral clustering," *Statistics and Computing.*, vol. 17, pp. 395–416, 2007.
- [60] J. Yang and J. Leskovec, "Overlapping community detection at scale: a nonnegative matrix factorization approach," in *Proc. ACM Int. Conf. Web Search Data Mining*, Rome, Feb. 2013, pp. 587–596.
- [61] J. Zhu, Y. Zhang, E. Levina, "Community detection in networks with node features," <http://arXiv:1509.01173>, 2015.
- [62] M. Vetterli and J. Kovačević, *Wavelets and Subband Coding*, Prentice Hall, Englewood Cliffs, NJ, 1995, <http://waveletsandsubbandcoding.org/>.
- [63] C. M. Bishop, *Pattern Recognition and Machine Learning*, Information Science and Statistics. Springer, 2006.
- [64] M. Ledoux, *The concentration of measure phenomenon*, vol. 89, Am. Math. Soc., 2001.
- [65] A. Singh, R. D. Nowak, and A. R. Calderbank, "Detecting weak but hierarchically-structured patterns in networks," in *Proc. Int. Conf. Artif. Intell. and Stat.*, 2010, pp. 749–756.
- [66] V. Kolmogorov and R. Zabih, "What energy functions can be minimized via graph cuts?," *IEEE Trans. Pattern Anal. Mach. Intell.*, vol. 26, no. 2, pp. 147–159, Feb. 2004.
- [67] D. Gleich, "The matlabgl matlab library," http://www.cs.purdue.edu/homes/dgleich/packages/matlab_bgl/index.html.
- [68] Y-L Zhang and F. Cao, "Fine particulate matter (pm2.5) in china at a city level," *Nature Sci. Reports*, 2015.
- [69] "Learn about air," <http://www.epa.gov/learn-issues/learn-about-air>.
- [70] "IEEE Xplore digital library," <http://ieeexplore.ieee.org/search/advsearch.jsp>.
- [71] J. L. Myers, A. D. Well, and R. F. Lorch Jr, *Research Design and Statistical Analysis*, Routledge, 2010.
- [72] P. Massart, *Concentration inequalities and model selection*, Springer-Verlag, 2007.

APPENDIX

A. Proof of Theorem 1

Under H_0^N , the observation is $\mathbf{y} = \text{Bernoulli}(\epsilon \mathbf{1}_V)$. Let the i th graph wavelet coefficient be

$$\begin{aligned} \mathbf{w}_i^T \mathbf{y} &= \sqrt{\frac{|S_1^{(i)}| |S_2^{(i)}|}{|S_1^{(i)}| + |S_2^{(i)}|}} \left(\frac{\mathbf{1}_{S_1^{(i)}}^T \mathbf{y}}{|S_1^{(i)}|} - \frac{\mathbf{1}_{S_2^{(i)}}^T \mathbf{y}}{|S_2^{(i)}|} \right) \\ &= \frac{\sqrt{|S^{(i)}|}}{2} \left(\frac{\mathbf{1}_{S_1^{(i)}}}{|S_1^{(i)}|} - \frac{\mathbf{1}_{S_2^{(i)}}}{|S_2^{(i)}|} \right)^T \mathbf{y}, \end{aligned}$$

where $S_1^{(i)}, S_2^{(i)}$ are two local child sets that form \mathbf{w}_i and $S^{(i)}$ is the parent local set. The second equality follows from the even partition. Since each element in \mathbf{y} is a Bernoulli random variable that takes value one with probability ϵ , the first term in the parentheses is the mean of $|S_1^{(i)}|$ Bernoulli random variables with success probability of ϵ . We then can show that

$$\mathbb{E} \left(\mathbf{1}_{S_1^{(i)}}^T \mathbf{y} / |S_1^{(i)}| \right) = |S_1^{(i)}| \epsilon / |S_1^{(i)}| = \epsilon.$$

Following from the Hoeffding inequality (Proposition 2.7 in [72]), for any η , $\mathbb{P} \left(\left| \mathbf{1}_{S_1^{(i)}}^T \mathbf{y} / |S_1^{(i)}| - \epsilon \right| \geq \eta \right) \leq 2e^{-2|S_1^{(i)}|\eta^2}$.

Thus, $(\mathbf{1}_{S_1^{(i)}}^T \mathbf{y} / |S_1^{(i)}| - \epsilon)$ is $1/(2\sqrt{|S_1^{(i)}|})$ -sub-Gaussian random variable. Combing two terms, we obtain that $\mathbf{w}_i^T \mathbf{y}$ is $\sqrt{2}/2$ -sub-Gaussian random variable. Then,

$$\mathbb{E} \left(\left\| \mathbf{W}_{(-1)}^T \mathbf{y} \right\|_{\infty} \right) = \mathbb{E} \left(\max_{2 \leq i \leq N} \mathbf{w}_i^T \mathbf{y} \right) \leq \sqrt{\log N}.$$

When $\text{var}(Z) = \sigma^2$, the Cirelson-Ibragimov-Sudakov inequality (Page 10 in [72]) ensures $\mathbb{P}(Z \geq \mathbb{E}Z + u) \leq e^{-u^2/2\sigma^2}$. Thus, with probability at least $1 - \delta_1$, we obtain

$$\begin{aligned} \hat{w} &= \left\| \mathbf{W}_{(-1)}^T \mathbf{y} \right\|_{\infty} \leq \mathbb{E} \left(\left\| \mathbf{W}_{(-1)}^T \mathbf{y} \right\|_{\infty} \right) + \sqrt{\log(1/\delta_1)} \\ &= \sqrt{\log N} + \sqrt{\log(1/\delta_1)}. \end{aligned} \quad (13)$$

In other words, when a threshold is $\tau = \sqrt{\log N} + \sqrt{\log(1/\delta_1)}$, the type-1 error is upper bounded by $1 - \delta_1$. This proves Lemma 3.

Under H_1^N , the observation is $\mathbf{y} = \text{Bernoulli}(\mu \mathbf{1}_C + \epsilon \mathbf{1}_V)$. We need to show there exists at least one wavelet basis vector capturing C well. We start with the following lemmas.

Lemma 6.

$$\left\| \mathbf{W}_{(-1)}^T \mathbf{1}_C \right\|_{\infty} \geq \sqrt{\frac{|C|(1 - |C|/N)}{1 + \rho \log N}}.$$

Proof.

$$\begin{aligned} \left\| \mathbf{W}_{(-1)}^T \mathbf{1}_C \right\|_{\infty} &\geq \frac{\left\| \mathbf{W}_{(-1)}^T \mathbf{1}_C \right\|_2^2}{\left\| \mathbf{W}_{(-1)}^T \mathbf{1}_C \right\|_0} \\ &\geq \frac{\left\| \mathbf{W}^T \mathbf{1}_C \right\|_2^2 - \left(\frac{1}{\sqrt{N}} \mathbf{1}_V^T \mathbf{1}_C \right)^2}{1 + \rho \log N} \\ &\geq \frac{\left\| \mathbf{1}_C \right\|_2^2 - |C|^2/N}{1 + \rho \log N} \geq \frac{|C|(1 - |C|/N)}{1 + \rho \log N}. \end{aligned}$$

The second inequality follows from Lemma 2 (Sparsity) in the paper with $\text{TV}_0(\mathbf{1}_C) \leq \rho$ and the even partition. \square

Let

$$\begin{aligned} i &= \arg \max_{2 \leq j \leq N} \mathbf{w}_j^T \mathbf{1}_C \\ &= \arg \max_{2 \leq j \leq N} \frac{\sqrt{|S^{(j)}|}}{2} \left(\frac{|S_1^{(j)} \cap C|}{|S_1^{(j)}|} - \frac{|S_2^{(j)} \cap C|}{|S_2^{(j)}|} \right), \end{aligned}$$

where $S_1^{(j)}, S_2^{(j)}$ are the children local sets of $S^{(j)}$. Following from Lemma 6,

$$\frac{\sqrt{S^{(i)}}}{2} \left(\frac{|S_1^{(i)} \cap C|}{|S_1^{(i)}|} - \frac{|S_2^{(i)} \cap C|}{|S_2^{(i)}|} \right) \geq \sqrt{\frac{|C|(1 - |C|/N)}{1 + \rho \log N}}. \quad (14)$$

Lemma 7. When $a \sim \text{Binomial}(n_1, p_1), b \sim \text{Binomial}(n_2, p_1)$, with probability $(1 - \delta)^2$,

$$|a + b - (n_1 p_1 + n_2 p_2)| \leq \sqrt{\frac{n_1}{2} \log\left(\frac{2}{\delta}\right)} + \sqrt{\frac{n_2}{2} \log\left(\frac{2}{\delta}\right)}.$$

Proof. Following from the Hoeffding inequality, with probability $1 - \delta$, $|a - n_1 p_1| \leq \sqrt{n_1 \log(2/\delta)}/2$. We bound both a and b , and rearrange the terms to obtain Lemma 7. \square

We aim to show that $|\mathbf{w}_i^T \mathbf{y}|$ is sufficiently large. Here, the term $\mathbf{1}_{S_1^{(i)}}^T \mathbf{y}$ counts how many ones appear inside the local set $S_1^{(i)}$ and is a random variable under the distribution of $\text{Binomial}(|S_1^{(i)} \cap C|, \mu) + \text{Binomial}(|S_1^{(i)} \cap \bar{C}|, \epsilon)$. Following Lemma 7, with probability $(1 - \delta)^2$,

$$\begin{aligned} & \left| \mathbf{1}_{S_1^{(i)}}^T \mathbf{y} - \left(|S_1^{(i)} \cap C| \mu + |S_1^{(i)} \cap \bar{C}| \epsilon \right) \right| \\ & \leq \sqrt{\frac{|S_1^{(i)} \cap C|}{2} \log\left(\frac{2}{\delta}\right)} + \sqrt{\frac{|S_1^{(i)} \cap \bar{C}|}{2} \log\left(\frac{2}{\delta}\right)}, \end{aligned}$$

where the similar formulation also holds for $S_2^{(i)}$. Without losing generality, we assume that $|S_1^{(i)} \cap C| \geq |S_2^{(i)} \cap C|$. With probability $(1 - \delta_2)^4$,

$$\begin{aligned} \mathbf{1}_{S_1^{(i)}}^T \mathbf{y} & \geq |S_1^{(i)} \cap C| \mu + |S_1^{(i)} \cap \bar{C}| \epsilon \\ & - \left(\sqrt{|S_1^{(i)} \cap C|} + \sqrt{|S_1^{(i)} \cap \bar{C}|} \right) \sqrt{\frac{1}{2} \log\left(\frac{2}{\delta_2}\right)}, \end{aligned}$$

where the similar formulation also holds for $S_2^{(i)}$. We have

$$\begin{aligned} |\mathbf{w}_i^T \mathbf{y}| & = \left| \frac{1}{\sqrt{|S^{(i)}|}} \left(\mathbf{1}_{S_1^{(i)}}^T \mathbf{y} - \mathbf{1}_{S_2^{(i)}}^T \mathbf{y} \right) \right| \\ & \geq \frac{|S_1^{(i)} \cap C| - |S_2^{(i)} \cap C|}{\sqrt{|S^{(i)}|}} (\mu - \epsilon) - \sqrt{2 \log\left(\frac{2}{\delta_2}\right)} \\ & \geq \sqrt{\frac{|C|(1 - |C|/N)}{1 + \rho \log N}} (\mu - \epsilon) - \sqrt{2 \log\left(\frac{2}{\delta_2}\right)}. \quad (15) \end{aligned}$$

The last inequality follows from (14). To simultaneously bound both type-1 and type-2 errors, the right hand side of (15) should be larger than the right hand side of (13). Thus, we obtain

$$\begin{aligned} \sqrt{|C| \left(1 - \frac{|C|}{N}\right)} (\mu - \epsilon) & \geq \sqrt{1 + \rho \log N} \left(\sqrt{\log N} + \sqrt{2 \log\left(\frac{2}{\delta_1}\right)} + \sqrt{2 \log\left(\frac{2}{\delta_2}\right)} \right), \end{aligned}$$

which proves Theorem 1.

B. Proof of Theorem 2

Under H_0^N , the observation is $\mathbf{y} = \text{Bernoulli}(\epsilon \mathbf{1}_V)$. Let $\mathcal{C} = \{C : \text{TV}_1(\mathbf{1}_C) \leq \rho\}$. Similarly to Lemma 4, by using the Hoeffding inequality, we can show that both $z_1(C) = \mathbf{1}_C^T (\mathbf{y} - \epsilon \mathbf{1}) / \sqrt{|C|}$ and $z_2 = \mathbf{1}^T (\mathbf{y} - \epsilon \mathbf{1}) / \sqrt{N}$ are sub-Gaussian random variables with mean zero and variance $1/2$. The graph scan statistic is then

$$\begin{aligned} \hat{g} & = \max_{C \in \mathcal{C}} |C| \text{KL} \left(\frac{\mathbf{1}_C^T \mathbf{y}}{|C|} \parallel \frac{\mathbf{1}^T \mathbf{y}}{N} \right) \\ & \leq 8 \max_{C \in \mathcal{C}} |C| \left(\frac{\mathbf{1}_C^T (\mathbf{y} - \epsilon \mathbf{1})}{|C|} - \frac{\mathbf{1}^T (\mathbf{y} - \epsilon \mathbf{1})}{N} \right)^2 \\ & = 8 \max_{C \in \mathcal{C}} \left(z_1(C) - \sqrt{\frac{|C|}{N}} z_2 \right)^2 \\ & = 8 \max \left[\left(\max_{C \in \mathcal{C}} \left(z_1(C) - \sqrt{\frac{|C|}{N}} z_2 \right) \right)^2, \right. \\ & \quad \left. \left(\min_{C \in \mathcal{C}} \left(z_1(C) - \sqrt{\frac{|C|}{N}} z_2 \right) \right)^2 \right] \end{aligned}$$

The random variable $z_1(C) - \sqrt{|C|/N} z_2$ is the difference between two sub-Gaussian random variables with same mean. The last equality takes care of both maximum and minimum. Since the distribution of $z_1(C) - \sqrt{|C|/N} z_2$ is symmetric and the tail probabilities on two sides are same, we only need to consider one side of the tail probability of $z_1(C) - \sqrt{|C|/N} z_2$.

Similarly to Theorem 5 in [45], we can show that with probability $1 - \delta_1$,

$$\begin{aligned} \max_{C \in \mathcal{C}} z_1(C) & \leq \left(\sqrt{\rho} + \sqrt{\frac{1}{2} \log N} \right) \sqrt{2 \log(N-1)} + \\ & \quad \sqrt{2 \log 2} + \sqrt{2 \log \frac{1}{\delta_1}}. \end{aligned}$$

Since z_2 is a sub-Gaussian random variable. $z_2 > -\sqrt{\log(2/\delta_1)}/2$ with probability $1 - \delta$. Finally, with probability at least $(1 - \delta_1)^2$, we have

$$\begin{aligned} \max_{C \in \mathcal{C}} \left(z_1(C) - \sqrt{\frac{|C|}{N}} z_2 \right) & \leq \sqrt{\frac{9}{2} \log \frac{2}{\delta_1}} + \\ & \left(\sqrt{\rho} + \sqrt{\frac{1}{2} \log N} \right) \sqrt{2 \log(N-1)} + \sqrt{2 \log 2}. \end{aligned}$$

Theorem 5 [45] is concerned with a Gaussian variable and here we are concerned with a sub-Gaussian variable. Thus, under the null hypothesis H_0^N , with probability $(1 - \delta_1)^2$,

$$\begin{aligned} \hat{g} & \leq 8 \left(\left(\sqrt{\rho} + \sqrt{\frac{1}{2} \log N} \right) \sqrt{2 \log(N-1)} + \sqrt{2 \log 2} + \sqrt{\frac{9}{2} \log(2/\delta_1)} \right)^2. \quad (16) \end{aligned}$$

In other words, when we set the threshold τ to be the right hand side of the above formula, the type-1 error is upper bounded by $(1 - \delta_1)^2$. This proves Lemma 4.

Under H_1^N , the observation is $\mathbf{y} = \text{Bernoulli}(\mu\mathbf{1}_C + \epsilon\mathbf{1}_{\bar{C}})$. *Proof.* Based on Lemma 7, with probability $(1 - \delta_2)^2$,

$$\left| \frac{\mathbf{1}^T \mathbf{y}}{N} - \epsilon - (\mu - \epsilon) \frac{|C|}{N} \right| \leq \sqrt{\frac{|C|}{2|N|^2} \log\left(\frac{2}{\delta_2}\right)} + \sqrt{\frac{N - |C|}{2N^2} \log\left(\frac{2}{\delta_2}\right)}.$$

Following from the Hoeffding inequality, with probability $1 - \delta$, $|\mathbf{1}_C^T \mathbf{y} / |C| - \mu| \leq \sqrt{\frac{1}{2|C|} \log(2/\delta_2)}$. Then, with probability $(1 - \delta_2)^3$,

$$\begin{aligned} \hat{g} &= \max_{C \in \mathcal{C}} |C| \text{KL} \left(\frac{\mathbf{1}_C^T \mathbf{y}}{|C|} \parallel \frac{\mathbf{1}^T \mathbf{y}}{N} \right) \\ &\geq \max_{C \in \mathcal{C}} |C| \left(\frac{\mathbf{1}_C^T \mathbf{y}}{|C|} - \epsilon - (\mu - \epsilon) \frac{|C|}{N} - \sqrt{\frac{1}{2N} \log(2/\delta_2)} \right)^2 \\ &\geq |C| \left(\frac{(N - |C|)(\mu - \epsilon)}{N} - \left(\sqrt{\frac{1}{2|C|}} + \sqrt{\frac{1}{2N}} \right) \sqrt{\log\left(\frac{2}{\delta_2}\right)} \right)^2. \end{aligned} \quad (17)$$

To simultaneously bound both type-1 and type-2 errors, the right hand side of (17) should be larger than the right hand side of (16). Thus, we obtain

$$\begin{aligned} \mu - \epsilon &\geq \frac{N}{N - |C|} \left(\frac{2\sqrt{2}}{\sqrt{|C|}} \left(\sqrt{2 \log 2} + \sqrt{\frac{9}{2} \log\left(\frac{2}{\delta_1}\right)} \right) \right. \\ &\quad \left. \left(\sqrt{\rho} + \sqrt{\frac{1}{2} \log N} \right) \sqrt{2 \log(N - 1)} \right) + \\ &\quad \left(\sqrt{\frac{1}{2|C|}} + \sqrt{\frac{1}{2N}} \right) \sqrt{\log\left(\frac{2}{\delta_2}\right)}. \end{aligned}$$

We can reformulate the above formula and obtain Theorem 2.

C. Proof of Theorem 3

Under H_0^N , the observation is $\mathbf{y} = \text{Bernoulli}(\epsilon\mathbf{1}_V)$. Let $\mathcal{X}_t = \{\mathbf{x} : \mathbf{x} \in [0, 1]^N, \text{TV}_1(\mathbf{x}) \leq \rho, \mathbf{1}^T \mathbf{x} \leq t\}$. Let $z_1(\mathbf{x}, t) = \mathbf{x}^T(\mathbf{y} - \epsilon\mathbf{1})/t$ and $z_2 = \mathbf{1}^T(\mathbf{y} - \epsilon\mathbf{1})/N$. The statistic is then

$$\begin{aligned} \hat{r} &= \max_{t, \mathbf{x} \in \mathcal{X}_t} t \text{KL} \left(\frac{\mathbf{x}^T \mathbf{y}}{t} \parallel \frac{\mathbf{1}^T \mathbf{y}}{N} \right) \\ &\leq 8 \max_{t, \mathbf{x} \in \mathcal{X}_t} t \left(\frac{\mathbf{x}^T(\mathbf{y} - \epsilon\mathbf{1})}{t} - \frac{\mathbf{1}^T(\mathbf{y} - \epsilon\mathbf{1})}{N} \right)^2 \\ &= 8 \max_{t, \mathbf{x} \in \mathcal{X}_t} \left(z_1(\mathbf{x}, t) - \sqrt{\frac{t}{N}} z_2 \right)^2 \\ &= 8 \max \left[\left(\max_{t, \mathbf{x} \in \mathcal{X}_t} \left(z_1(\mathbf{x}, t) - \sqrt{\frac{t}{N}} z_2 \right) \right)^2, \right. \\ &\quad \left. \left(\min_{t, \mathbf{x} \in \mathcal{X}_t} \left(z_1(\mathbf{x}, t) - \sqrt{\frac{t}{N}} z_2 \right) \right)^2 \right] \end{aligned}$$

The last equality takes care of both maximum and minimum. Since the distribution of $z_1(\mathbf{x}, t) - \sqrt{t/N} z_2$ is symmetric, we only need to consider one side of the distribution.

Lemma 8.

$$\mathbb{E}_{\mathbf{y}} \max_{t, \mathbf{x} \in [0, 1]^N, \mathbf{1}^T \mathbf{x} \leq t} z_1(\mathbf{x}, t) \leq \sqrt{\frac{N \log 2}{2}}.$$

$$\begin{aligned} &\mathbb{E}_{\mathbf{y}} \max_{t, \mathbf{x} \in [0, 1]^N, \mathbf{1}^T \mathbf{x} \leq t} \frac{\mathbf{x}^T(\mathbf{y} - \epsilon\mathbf{1})}{\sqrt{t}} \\ &= \mathbb{E}_{\mathbf{y}} \max_t \frac{1}{\sqrt{t}} \max_{\mathbf{x} \in [0, 1]^N, \mathbf{1}^T \mathbf{x} \leq t} \mathbf{x}^T(\mathbf{y} - \epsilon\mathbf{1}) \\ &= \mathbb{E}_{\mathbf{y}} \max_t \frac{1}{\sqrt{t}} \max_{\mathbf{x} \in \{0, 1\}^N, \mathbf{1}^T \mathbf{x} \leq t} \mathbf{x}^T(\mathbf{y} - \epsilon\mathbf{1}) \\ &= \mathbb{E}_{\mathbf{y}} \max_{\mathbf{x} \in \{0, 1\}^N} \frac{\mathbf{x}^T(\mathbf{y} - \epsilon\mathbf{1})}{\sqrt{\mathbf{1}^T \mathbf{x}}}. \end{aligned}$$

When \mathbf{x} is a binary variable, $\mathbf{x}^T(\mathbf{y} - \epsilon\mathbf{1})/\sqrt{\mathbf{1}^T \mathbf{x}}$ is a 1/2-sub-Gaussian random variable as shown previously. The cardinality of the set $\{0, 1\}^N$ is 2^N . Thus,

$$\mathbb{E}_{\mathbf{y}} \max_{t, \mathbf{x} \in [0, 1]^N, \mathbf{1}^T \mathbf{x} \leq t} \frac{\mathbf{x}^T(\mathbf{y} - \epsilon\mathbf{1})}{\sqrt{t}} \leq \sqrt{\frac{1}{2} \log 2^N}.$$

□

Combining Lemma 8 and to Theorem 5 in [45], we can show that with probability $1 - \delta_1$,

$$\begin{aligned} \max_{t, \mathbf{x} \in \mathcal{X}_t} z_1(\mathbf{x}, t) &\leq \frac{\log 2N + 1}{\sqrt{\left(\sqrt{\rho} + \sqrt{\frac{1}{2} \log N} \right)^2 \log N}} \\ &\quad + 2 \sqrt{\left(\sqrt{\rho} + \sqrt{\frac{1}{2} \log N} \right)^2 \log N + \sqrt{2 \log 2} + \sqrt{2 \log \frac{1}{\delta_1}}}. \end{aligned}$$

Since z_2 is a sub-Gaussian random variable. $z_2 > -\sqrt{\log(2/\delta_1)}/2$ with probability $1 - \delta_1$. Finally, with probability at least $(1 - \delta_1)^2$, we have

$$\begin{aligned} &\max_{t, \mathbf{x} \in \mathcal{X}_t} \left(z_1(\mathbf{x}, t) - \sqrt{\frac{t}{N}} z_2 \right) \\ &\leq \frac{\log 2N + 1}{\sqrt{\left(\sqrt{\rho} + \sqrt{\frac{1}{2} \log N} \right)^2 \log N}} + \sqrt{2 \log 2} \\ &\quad + 2 \sqrt{\left(\sqrt{\rho} + \sqrt{\frac{1}{2} \log N} \right)^2 \log N + \sqrt{\frac{9}{2} \log \frac{2}{\delta_1}}}. \end{aligned}$$

Thus, under the null hypothesis H_0^N , with probability $(1 - \delta_1)^2$,

$$\begin{aligned} \hat{r} &\leq 8 \left(\frac{\log 2N + 1}{\sqrt{\left(\sqrt{\rho} + \sqrt{\frac{1}{2} \log N} \right)^2 \log N}} + \sqrt{2 \log 2} \right. \\ &\quad \left. + 2 \sqrt{\left(\sqrt{\rho} + \sqrt{\frac{1}{2} \log N} \right)^2 \log N + \sqrt{\frac{9}{2} \log\left(\frac{2}{\delta_1}\right)}} \right)^2 \end{aligned} \quad (18)$$

In other words, when we set the threshold τ to be the right hand side of the above formula, the type-1 error is upper bounded by $(1 - \delta_1)^2$. This proves Lemma 5.

Under H_1^N , the observation is $\mathbf{y} = \text{Bernoulli}(\mu\mathbf{1}_C + \epsilon\mathbf{1}_{\bar{C}})$. Let $t^* = |C|$, $\mathbf{x}^* = \mathbf{1}_C$. Similarly to the proof in Theorem 2, with probability at least $(1 - \delta_2)^3$,

$$\begin{aligned}
\hat{r} &= t^* \text{KL} \left(\frac{\mathbf{y}^T \mathbf{x}^*}{t^*} \parallel \frac{\mathbf{1}^T \mathbf{y}}{N} \right) = |C| \text{KL} \left(\frac{\mathbf{1}_C^T \mathbf{y}}{|C|} \parallel \frac{\mathbf{1}^T \mathbf{y}}{N} \right) \\
&\geq |C| \left(\frac{N - |C|}{N} (\mu - \epsilon) - \left(\sqrt{\frac{1}{2|C|}} + \sqrt{\frac{1}{2N}} \right) \sqrt{\log\left(\frac{2}{\delta_2}\right)} \right)^2.
\end{aligned} \tag{19}$$

To simultaneously bound both type-1 and type-2 errors, the right hand side of (19) should be larger than the right hand side of (18). Thus, we obtain

$$\begin{aligned}
\mu - \epsilon &\geq \frac{N}{N - |C|} \left(\frac{2\sqrt{2}}{\sqrt{|C|}} \left(\frac{\log 2N + 1}{\sqrt{\left(\sqrt{\rho} + \sqrt{\frac{1}{2} \log N}\right)^2 \log N}} \right. \right. \\
&\quad \left. \left. + \sqrt{2 \log 2} + 2 \sqrt{\left(\sqrt{\rho} + \sqrt{\frac{1}{2} \log N}\right)^2 \log N + \sqrt{\frac{9}{2} \log\left(\frac{2}{\delta_1}\right)}} \right) \right. \\
&\quad \left. + \left(\sqrt{\frac{1}{2|C|}} + \sqrt{\frac{1}{2N}} \right) \sqrt{\log\left(\frac{2}{\delta_2}\right)} \right);
\end{aligned}$$

We can reformulate the above formula and obtain Theorem 3.

D. Naive Approach

As mentioned in Section IV-B, a naive statistic is to compute the average value $\hat{n} = \mathbf{1}_V^T \mathbf{y}$.

Theorem 4. The sufficient condition to distinguish H_1^N from H_0^N by the average statistic is

$$|C|(\mu - \epsilon) \geq O(\sqrt{N}).$$

Proof. Using Hoeffding inequality, we can show that under H_0^N , $\mathbb{P}(|\mathbf{1}^T \mathbf{y}/N - \epsilon| \geq \eta) \leq 2e^{-2N\eta^2}$, for any η , while under H_1^N , $\mathbb{P}(|\mathbf{1}^T \mathbf{y}/N - (\mu|C| + \epsilon(N - |C|))/N| \geq \eta) \leq 2e^{-2N\eta^2}$, for any η . Thus, when $|C|(\mu - \epsilon) \geq \sqrt{(N/2) \log(2/\delta)}$ we have that $\mathbb{P}\{T = 1 | H_0^N \text{ is true}\} \leq \delta$ and $\mathbb{P}\{T = 0 | H_1^N \text{ is true}\} \geq 1 - \delta$. \square

We thus see that the sufficient condition in Theorem 4 is much looser than the sufficient conditions in Theorems 1 and 2, indicating that the proposed approaches are provably better than this naive approach.